

# RSC Advances



This is an *Accepted Manuscript*, which has been through the Royal Society of Chemistry peer review process and has been accepted for publication.

*Accepted Manuscripts* are published online shortly after acceptance, before technical editing, formatting and proof reading. Using this free service, authors can make their results available to the community, in citable form, before we publish the edited article. This *Accepted Manuscript* will be replaced by the edited, formatted and paginated article as soon as this is available.

You can find more information about *Accepted Manuscripts* in the [Information for Authors](#).

Please note that technical editing may introduce minor changes to the text and/or graphics, which may alter content. The journal's standard [Terms & Conditions](#) and the [Ethical guidelines](#) still apply. In no event shall the Royal Society of Chemistry be held responsible for any errors or omissions in this *Accepted Manuscript* or any consequences arising from the use of any information it contains.

## Ternary dyes adsorption onto MnO<sub>2</sub> nanoparticle-loaded activated carbon: derivative spectrophotometry and modeling

Arash Asfaram <sup>a</sup>, Mehrorang Ghaedi<sup>1a</sup>, Shaaker Hajati <sup>b</sup>, Alireza Goudarzi <sup>c</sup>

<sup>a</sup> *Chemistry Department, Yasouj University, Yasouj 75918-74831, Iran.*

<sup>b</sup> *Department of Physics, Yasouj University, Yasouj 75918-74831, Iran*

<sup>c</sup> *Department of Polymer Engineering, Golestan University, Gorgan, 49188-88369, Iran*

RSC Advances Accepted Manuscript

---

1 Corresponding author at: Tel.: +98 741 2223048; fax: +98 741 2223048.  
E-mail address: [m\\_ghaedi@mail.yu.ac.ir](mailto:m_ghaedi@mail.yu.ac.ir); [m\\_ghaedi@yahoo.com](mailto:m_ghaedi@yahoo.com) (M. Ghaedi)

## Abstract

The MnO<sub>2</sub> nanoparticle-loaded activated carbon (MnO<sub>2</sub>-NP-AC) as an efficient, environmental friendly and cost-effective adsorbent was simply synthesized and characterized using different techniques such as FE-SEM, EDX, XRD, BET and FTIR. The rapid and simultaneous ultrasound-assisted adsorption of brilliant green (BG), crystal violet (CV) and methylene blue (MB) dyes with severe spectra overlap was investigated onto MnO<sub>2</sub>-NP-AC as a novel and efficient adsorbent. The dyes in their ternary mixtures were simultaneously determined using third order derivative spectrophotometry. Response surface methodology (RSM) was successfully applied to analyze and optimize the adsorption process. The optimal conditions for pH, adsorbent dosage, initial dyes concentration and sonication time were obtained to be 7.0, 0.022 g, 6 mg L<sup>-1</sup> and 4 min, respectively. Predicted and experimental data were found to be in good agreement. Artificial neural network (ANN) was applied for the accurate prediction of percentages of dyes removal from their ternary solution by MnO<sub>2</sub>-NP-AC adsorbent.

The experimental equilibrium data were modeled by applying different isotherm models. The Langmuir model was found to be the most applicable one for describing the experimental equilibrium data obtained at optimal condition. A small amount of MnO<sub>2</sub>-NP-AC adsorbent (0.005 g) was successfully used for the removal of dyes (RE > 90.0%) in very short time (4.0 min) with high adsorption capacity in single component system (206.20, 234.20 and 263.16 mg g<sup>-1</sup> for BG, CV and MB, respectively). Kinetics study showed the applicability of the second-order kinetic model.

**Keywords:** Artificial neural network, Brilliant green, Crystal Violet, Methylene blue, MnO<sub>2</sub>-NP-AC, Response surface methodology.

## 1. Introduction

Because of the extensive use of dye stuffs in human life, the related industries are being expanded rapidly.<sup>1</sup> Many synthetic dyes are toxic and carcinogenic which are not easily degraded to safe concentrations in the environment.<sup>2</sup>

Methylene blue (MB) (Fig 1a) as a thiazine cationic dye is commonly used for coloring paper and hair,<sup>3</sup> dyeing of cotton, wood, and silk.<sup>4</sup> Although MB is not highly hazardous; it can cause some harmful effects in humans such as increased heart rate, shock, vomiting, jaundice, cyanosis, quadriplegia, and tissue necrosis.<sup>4</sup>

Brilliant green (BG) (Fig 1b) is one of the most important dyes within the category of dye stuffs, which has been extensively used for dyeing silk, wool, leather, jute, cotton, biological stain, dermatological agent, veterinary medicine, green ink manufacture, intestinal parasites, fungus textile dyeing and paper printing. Therefore, wastewater of these industries is highly colored and causes water pollution which should be treated before its disposal.<sup>5</sup>

As a typical cationic dye, Crystal violet (CV) (Fig 1c) belongs to triphenylmethane group which is widely applied in coloring paper, temporary hair colorant, dyeing cottons, and wools. CV may harm the body via inhalation, ingestion and skin contact. It has also been found to cause cancer and severe eye irritation to human beings.<sup>6, 7</sup> Therefore, it is very essential to remove BG, CV and MB from industrial effluents.

Various techniques, such as adsorption and biosorption,<sup>8-13</sup> membrane process,<sup>4</sup> coagulation,<sup>14</sup> flocculation,<sup>15</sup> photo decomposition,<sup>16</sup> electrochemical oxidation,<sup>17</sup> have been used for the removal of dyes from wastewater. Among these techniques, adsorption has been proven to be the most potential one due to its flexibility, simplicity of design, high efficiency and ability to separate wide range of chemical compounds.<sup>18</sup>

Nanoparticle-based adsorbents with distinguished properties including high number of vacant reactive surface sites, metallic or semi-metallic behavior and high surface area have been applied for the removal of various toxic materials.<sup>19-21</sup> The MnO<sub>2</sub>- nanoparticles, as unique adsorbent, benefit from their high specific surface area which makes it suitable for pollutants removal.

For modeling the absorption process, response surface methodology (RSM) and artificial neural network (ANN) as the most popular methods are employed.<sup>22-24</sup> RSM and ANN are applied for systems where the mathematical relationship between the parameters and the responses is

unknown. Both tools are able to capture and represent complex nonlinear relationships between independent variables and responses of the system.

The main objectives of the present study include the following:

- (1) The synthesis of  $\text{MnO}_2$  nanoparticle-loaded activated carbon ( $\text{MnO}_2\text{-NP-AC}$ ) and characterization of it by FESEM, EDX, XRD, BET and FTIR.
- (2) Determination of dyes concentrations by derivative spectrophotometry in ternary system.
- (3) The design and optimization of experiments using RSM as a statistical approach to maximize the efficiency of dyes adsorption.
- (4) Ultrasound-assisted adsorption as a simple, inexpensive, rapid and sensitive method followed by derivative spectrophotometry applied for the simultaneous removal of CV, BG and MB.
- (5) The evaluation of suitable isotherm and kinetic models describing the adsorption process, and finally,
- (6) The application of ANN model for inspection of nonlinear relationships between variables.

## 2. Experimental

### 2.1. Instruments and reagents

Fig. 1 shows the chemical structure of CV ( $\text{C}_{25}\text{N}_3\text{H}_{30}\text{Cl}$ ), BG ( $\text{C}_{27}\text{H}_{34}\text{N}_2\text{O}_4\text{S}$ ) and MB ( $\text{C}_{16}\text{H}_{18}\text{N}_3\text{SCl}$ ) dyes. The maximum absorbance of CV, BG and MB occurs at wavelengths of 584, 624 and 664 nm, respectively. The stock solutions ( $100 \text{ mg L}^{-1}$ ) were prepared by dissolving 10 mg of each dye in 100 mL double distilled water. The test solutions ( $5\text{--}40 \text{ mg L}^{-1}$ ) were prepared daily by diluting their stock solutions with distilled water. All applied chemicals (analytical reagent grade) were supplied from Merck, Darmstadt, Germany.

Manganese sulfate dehydrate ( $\text{MnSO}_4 \cdot 2\text{H}_2\text{O}$ ), purchased from Merck Company, was used as manganese ion source without further purification. Ammonia solution (25 % w/w) was provided from Chem. lab Company and used as received without further purification.

Distilled water was used in all experiments. The absorbance spectra were recorded by a Jasco UV-vis spectrophotometer model V-530. A HERMLE Labortechnik GmbH centrifuge model Z206A (Germany) was used to accelerate the phase separation. A Metrohm digital pH-meter model 686 (Switzerland) with a combined Ag/AgCl glass electrode was used for pH adjustments. The elemental composition of the  $\text{MnO}_2\text{-NP-AC}$  was analyzed by energy-dispersive X-ray spectrometer (EDX) using an Oxford INCA II energy solid state detector. X-ray diffraction

(XRD, Philips PW 1800) was performed to characterize the phase and structure of the prepared nanoparticles using  $\text{Cu}_{k\alpha}$  radiation (40 KV and 40 mA) at angles ranging from 10 to 80°. The morphology of the nanoparticles was observed by field emission scanning electron microscopy (FESEM: ZEISS) under an acceleration voltage of 15 KV. To investigate the purity as well as the presence of organic and/or other compounds in the nanoparticles, a Fourier transform infrared (FT-IR) spectrum was recorded using a Perkin Elmer-Spectrum RX-IFTIR spectrometer in the range of 300–4000  $\text{cm}^{-1}$ . An ultrasonic bath with heating system (Tecno-GAZ SPA Ultra Sonic System) at frequency of 40 kHz and power of 130 W was used for the ultrasound-assisted adsorption procedure. A BET surface analyzer (PHS-1020(PHSCINA)) was used to measure nitrogen adsorption–desorption isotherm at 77 K while before the measurement, the samples were degassed using nitrogen gas at 553 K for 3 h. The BET surface area was obtained from the adsorption isotherms. The STATISTICA software version 10.0 (Stat Soft Inc., Tulsa, USA) was used for the design of experiments and their subsequent statistical analysis.

### 2.2. Derivative spectrophotometric method

The standard solutions of ternary mixtures were prepared from their individual stock solutions (100 mg  $\text{L}^{-1}$ ). The pH of the ternary mixtures was adjusted by using HCl and NaOH solutions. The zero order spectra were obtained between 350 and 750 nm with  $\Delta\lambda$  and scan speed of 1 nm and 1920  $\text{nm min}^{-1}$ , respectively. Before each differentiation step, Savitzky–Golay smoothing procedure<sup>25</sup> was applied to improve the signal-to-noise and thus to obtain more reliable quantification by using derivative spectra. The  $\lambda$  values from the third order derivative spectra for the determination of the individual dyes were selected from the zero-crossing technique.

### 2.3. Preparation of $\text{MnO}_2$ -NPs loaded on AC

The reaction solution for the fabrication of  $\text{MnO}_2$ -NP-AC was prepared as follows: first 12.5 g of activated carbon (AC) was mixed with 200 mL of 0.0125 mol  $\text{L}^{-1}$  manganese sulfate solution as a deposition suspension solution in an Erlenmeyer flask. Then 10 mL of a fresh ammonia solution (25 % w/w), diluted by adding 50 mL distilled water, was added drop by drop to the deposition solution while strongly stirred for 5 minutes at temperature of 30 °C. After adding diluted ammonia solution to deposition solution, the mixed solution was strongly stirred for 21 hours at room temperature to deposit  $\text{MnO}_2$ -NPs on activated carbon, homogenously. In the next

step, the suspension solution of MnO<sub>2</sub>-NP-AC was heated at 65 °C for one hour. Then it was filtered and washed several times by distilled water followed by drying at 60 °C for 3h. Finally, it was characterized and used as an efficient absorbent for the simultaneous adsorption of CV, BG and MB.

#### 2.4. *Ultrasound-assisted adsorption*

The simultaneous adsorption of CV, BG and MB was accelerated using ultrasound, while the ultrasonic bath was filled with 2.5 L water (the sonication medium) at 25 °C during the experiment. The sonochemical adsorption experiment was undertaken as follows: 50 mL of dyes solution at known concentration (initial concentration of 6 mg L<sup>-1</sup> for each dye) and a known amount of MnO<sub>2</sub>-NP-AC (0.022 g) were loaded into the flask and kept at the desired sonication time (4 min) at pH 7.0 and at room temperature. Finally, the sample was immediately centrifuged and solutions were analyzed for the final concentration of CV, BG and MB via derivative spectrophotometric method at 550, 440 and 710 nm, respectively. The amount of each dye was analyzed via the corresponding calibration curve at the mentioned wavelength. In ternary solutions, the third order derivative of the absorbance spectra was used to find the optimal wavelength for each dye at which the impact of the other component was minimized. The optimal wavelengths were found to be 550, 440 and 710 nm for CV, BG and MB respectively.

#### 2.5. *Measurements of dye uptake*

The dyes concentrations were determined according to calibration plots. The CV, BG and MB removal percentages (R %) were calculated using the following equation:

$$R\% = \frac{C_0 - C_t}{C_0} \times 100\% \quad (1)$$

where C<sub>0</sub> (mg L<sup>-1</sup>) and C<sub>t</sub> (mg L<sup>-1</sup>) are the dye concentration at initial time and after time t, respectively. The equilibrium adsorption capacity of each dye was calculated from the following equation:

$$q_e = \frac{(C_0 - C_e)V}{W} \quad (2)$$

where  $C_0$  ( $\text{mg L}^{-1}$ ) and  $C_e$  ( $\text{mg L}^{-1}$ ) are the initial and equilibrium dye concentrations in solution, respectively,  $V$  (L) is the volume of the solution and  $W$  (g) is the mass of the adsorbent.

The kinetic studies were performed in a series of flask containing 0.010 g of  $\text{MnO}_2$ -NP-AC and 50 mL of each dye of concentration of 10, 20 and 30  $\text{mg L}^{-1}$  at room temperature. After fixed time intervals (1-5 min), the adsorbent was separated and the concentration of each dye remaining in the supernatant solution was determined by a UV-Visible spectrophotometry at its  $\lambda_{\text{max}}$ . The isotherm parameters were also obtained in the initial dyes concentrations range of 5–30  $\text{mg L}^{-1}$  in 50 mL of each solution mixed with 0.005, 0.010, 0.015 and 0.022 g of  $\text{MnO}_2$ -NP-AC at pH 7.0 for 4.0 min sonication time.

To quantitatively compare the applicability of each model, an error function is required. As a result, a Chi-square ( $\chi^2$ ) test and the coefficient of determination ( $R^2$ ) were employed as criteria to obtain the best isotherm and kinetic models for describing the experimental equilibrium data in non-linear regression analysis.<sup>26</sup>

The following non-linear chi-square test ( $\chi^2$ )<sup>27</sup> was carried out on the best-fitted isotherm:

$$\chi^2 = \sum \frac{(q_{e,\text{exp}} - q_{e,\text{cal}})^2}{q_{e,\text{cal}}} \quad (3)$$

where  $q_{e,\text{exp}}$  and  $q_{e,\text{cal}}$  are experimental and calculated adsorption capacities, respectively. A small value of  $\chi^2$  indicates that the data obtained from the model is consistent to the experimental value.

## 2.6. Experimental design

Response surface methodology (RSM), which resulted from the combination of both mathematical and statistical methods, is advantageous to be used for the demonstration and optimization of the influences of a number of independent variables on the response.<sup>28</sup> RSM is very useful to reduce the number of experiments to be conducted, in order to produce adequate information, which is statistically acceptable as a result.<sup>29, 30</sup> RSM usually contains three steps:



(1) design and experiments; (2) response surface modeling through regression; (3) optimization.

<sup>31</sup> The most popular design of experiment applied in RSM technique is central composite design (CCD). CCD has following three sets of experimental runs: (1) Fractional factorial runs in which factors are studied at +1, -1 levels, (2) Center points, and (3) Axial points which make the design rotatable.<sup>31</sup>

The center points are used to determine the experimental error and the reproducibility of the data. The axial points are located at  $(\pm\alpha, 0, 0)$ ,  $(0, \pm\alpha, 0)$  and  $(0, 0, \pm\alpha)$  where  $\alpha$  is the distance of the axial point from center. In this study,  $\alpha$  value was fixed at 2.8284.<sup>32</sup>

Based on this method a six-factor design was considered for the removal of dyes. These factors include pH ( $X_1$ ), Adsorbent dosage ( $X_2$ ), Sonication time ( $X_3$ ), MB concentration ( $X_4$ ), BG concentration ( $X_5$ ) and CV concentration ( $X_6$ ) in five coded levels (-2.8284, -1, 0, +1 and +2.8284). The most common model which is used to describe the relationship between vital input factors and measurable output is the quadratic regression model which can be expressed as follows:<sup>33</sup>

$$y = \beta_0 + \sum_{i=1}^k \beta_i X_i + \sum_{i=1}^k \sum_{j=1}^k \beta_{ij} X_i X_j + \sum_{i=1}^k \beta_{ii} X_i^2 + \varepsilon \quad (4)$$

where  $y$  represents the process response or output (i.e., dependent variable),  $k$  is the number of factors,  $i$  and  $j$  are index numbers for factors,  $\beta_0$  is the free term (i.e., offset term),  $X_1 \dots X_k$  are coded independent variables,  $\beta_i$  is the coefficient of first-order effect (i.e., linear, primary effect),  $\beta_{ii}$  is the quadratic effect (i.e. squared effect),  $\beta_{ij}$  represents the interaction effect, and  $\varepsilon$  is the random error accounting for the discrepancies or uncertainties between predicted and observed values.

### 2.7. Definition of the ANN modeling

Artificial neural network (ANN) is a good inspiration of human brain and nerve systems that are known for their extreme ability to learn and classify data.<sup>34</sup> A three layer feed-forward ANN was established for modeling purpose. The network contains an input layer, a hidden layer and an output layer. Each layer consists of a series of neurons (Fig. 2). Neurons transfer input values to next layer that the strength of these connections is determined by weights.<sup>35</sup> In the present study,

different back-propagation (BP) algorithms were checked to select the best BP algorithm with a minimum mean squared error (MSE) and minimum relative error (MRE). The Levenberg–Marquardt back propagation algorithm (LMA) was applied for training the network as the best algorithm. Also, a three-layer feed forward ANN with a linear transfer function (purelin) at output layer and with a tangent sigmoid transfer function (tansig) at hidden layer was developed to predict and simulate MnO<sub>2</sub>-NP-AC adsorption capacity for dyes removal. For ternary solution, all experimental data (90 runs) were divided randomly into three groups (70 % for training, 15 % for cross validation and 15 % for testing the accuracy of model and prediction). The criteria such as absolute average deviation (AAD), mean squared error (RMS), mean absolute error (MAE) and the correlation coefficient ( $R^2$ ) were applied to evaluate the performance of the ANN model. The training parameters were 6 input nodes, 15 hidden layer neurons, 3 output node and error goal of 0.0002. Sensitivity analysis was carried out to compare the relative importance of each input variable. All the calculations involved were conducted using MATLAB.

### 3. Results and discussion

#### 3.1. Simultaneous analysis of CV, BG and MB in ternary mixtures

Fig. 3a shows the zero order spectra of CV, BG, MB and their ternary mixture. The maximum wavelengths ( $\lambda_{\max}$ ) appear at 584, 624 and 644 nm for CV, BG, and MB, respectively. The individual spectra of these three dyes overlap severely, which is not possible to determine their accurate concentrations in the ternary mixture using conventional method. To solve this overlap problem and determine the dyes simultaneously, the third order derivatives of the spectra were obtained as shown in Figs. 3b and 3c. The third order derivative spectra show that CV can be determined at 550 nm where the impacts of BG and MB are trivial. At 440 nm, BG can be determined, whereas the absorbances of CV and MB are equal to zero. At 710 nm, no trace of the BG and CV is observed and thus the absorbance at this wavelength is attributed to MB. In order to test the mutual independence of the analytical signals of CV, BG and MB, calibration graphs were constructed for standard solutions containing various amounts of CV, BG and MB. The similarity observed between regression equations of individual dyes and their mixed solution suggested no interference in the estimation of one dye in the presence of the other. The regression equations and coefficients of determinations of the calibration graphs are given in Table 1. The derivative amplitudes measured at 550 nm for CV were found to be independent of

the concentrations of BG and MB. Similarly, derivative amplitudes measured at 440 and 710 nm for BG and MB were found to be independent of the concentration of CV. The validity of the proposed method was determined in several synthetic ternary mixtures containing CV, BG and MB.

### 3.2. Characterization of adsorbent

The size and morphology of the MnO<sub>2</sub>-NP-AC were investigated by field emission scanning electron microscopy. FE-SEM image shows the sheet-like morphology of the MnO<sub>2</sub>-NP-AC with thickness of about 50-100 nm. Many spherical-like nanoparticles with diameters of about 20-50 nm were also observed (Fig. 4a).

The results for the determination of pH<sub>ZPC</sub> of MnO<sub>2</sub>-NP-AC were illustrated in Fig. 4b. The surface of MnO<sub>2</sub>-NP-AC is neutral when pH of the aqueous solution is equal to pH<sub>ZPC</sub> (2.0). At pH < 2.0, the adsorbent surface is positively charged that may be due to the accumulation of H<sub>3</sub>O<sup>+</sup> ions into adsorbent functional groups e.g. hydroxyl group or donating nitrogen atom. Thus, a repulsive force occurs between the cationic dyes and the adsorbent surface, which causes a decrease in the adsorption percentage. On the other way, at pH > pH<sub>ZPC</sub>, the adsorbent surface is negatively charged due to the deprotonation of its functional group that causes an increase in the adsorption percentage.

The BET surface area of MnO<sub>2</sub>-NP-AC was determined to be 612.03 m<sup>2</sup> g<sup>-1</sup>. The adsorbent was found to be mesoporous with average pore diameter of 2.52 nm. The adsorption-desorption isotherm was studied using nitrogen as adsorptive gas (Fig. 4c). As seen, the isotherm is of type V which is characteristic of a mesoporous material.

The chemical composition of the MnO<sub>2</sub>-NP-AC was studied by EDX analysis from which the presence of Mn and O in the sample was confirmed (Fig. 5(a)). The Au peak is related to gold coated by sputtering required for FE-SEM image acquisition. In EDX analysis (Fig. 5(a)), C, O and Mn are the dominant elements throughout the surface of the MnO<sub>2</sub>-NP-AC with weight percentages of 90.00 %, 4.80 %, and 5.10 %, respectively. 61.87 % of oxygen present in the sample has been contributed in MnO<sub>2</sub> nanoparticles and 38.13 % of which may be attributed to oxygen-containing functional groups present at the surface of activated carbon.

Fig. 5(b) shows the XRD pattern of the MnO<sub>2</sub>-NP-AC particles. The observed broad hump at 2θ=20-25° as well as a broad peak at 2θ=43° is related to the amorphous nature of activated carbon particles on which the MnO<sub>2</sub> nanoparticles were loaded. Therefore, according to the

obtained XRD pattern the prepared MnO<sub>2</sub>-NPs had an amorphous structure. Fig. 5(c) shows FT-IR spectrum of the prepared MnO<sub>2</sub> nanoparticles in the range of 300–4000 cm<sup>-1</sup>. FTIR spectroscopy was carried out in order to investigate the purity as well as the presence of organic and/or other compounds in MnO<sub>2</sub> nanoparticles. Hydroxides and oxides of metal nanoparticles usually give the absorption peak in the finger print region i.e. below wavelength of 1000 cm<sup>-1</sup> arising from inter-atomic vibrations. An strong and sharp peak at 586 cm<sup>-1</sup> in the spectrum is due to Mn–O vibrations modes in MnO<sub>2</sub>.<sup>36</sup> Jaganyi *et al*<sup>37</sup> reported an absorption peak at 475 cm<sup>-1</sup> corresponding to the characteristic stretching collision of O–Mn–O and thus, the peak observed at 458 cm<sup>-1</sup> is attributed to O–Mn–O bond. Broad absorption peaks centered around 3381 cm<sup>-1</sup> and 1610 cm<sup>-1</sup> are raised by the absorbed water molecules and carbon dioxide because the nanocrystalline materials exhibit a high surface-to-volume ratio.<sup>38</sup> X. Chu *et al.* reported an absorption peak for the Mn-OH functional group at 1109 cm<sup>-1</sup>, while in the FTIR spectrum of the MnO<sub>2</sub> nanoparticles prepared in this work, no absorption peak related to the Mn-OH functional group was observed.

### 3.3. CCD results and fitted regression equations associated to the total surface area

The CCD under RSM was employed to evaluate the interaction among the significant variables and also to determine their optimal values. The CCD was developed to use the least number of experimental runs and increase the efficiency. The CCD has been applied and considered to be a very efficient statistical experimental design tool in optimization.<sup>30</sup>

The coded and real values of the factors are shown in Table 2. The experimental conditions for batch runs and the corresponding responses (removal percentages of the dyes) are shown in Table 3.

Full quadratic polynomial models were applied for all responses (see Table 4 for statistical parameters). A linear relationship between the experimental and predicted values of the responses was observed as shown in Fig. 6a with high correlation coefficient that indicates the applicability of models. Guan and Yao<sup>39</sup> suggested that R<sup>2</sup> should be at least 0.80 for the good fit of a model. In this case, R<sup>2</sup> of the model obtained was 0.993, 0.997 and 0.987 for BG, MB and CV, respectively.

Table 5 summarizes the results obtained for the ANOVA study. The statistical significance of the model is determined by F-test ANOVA. A p-value less than 0.05 implies the significance of the

corresponding variable.<sup>28</sup> The independent parameters including pH, adsorbent dosage, sonication time and initial concentration of each dye have a significant influence on the yield of the adsorption (Table 5).

The non-significant value of lack of fit and a significant value for model proved the validity of the quadratic model. This model for RSM proved to be highly significant due to its high Fisher's F-value (711, 322 and 175 for BG, MB and CV, respectively) with a low probability value ( $p < 0.0001$ ) (Table 5). The predicted R-squared (0.981, 0.990 and 0.995 for CV, BG and MB, respectively) and the adjusted R-squared (0.969, 0.983 and 0.992 for CV, BG and MB, respectively) are in reasonable agreement. The residual variation is measured using coefficient of variance relative to the size of the mean. A very low value of coefficient of variance (0.929, 0.582 and 1.15 for BG, MB and CV, respectively) implies a sufficient precision and reliability of the experimental results. Predicted residual sum of squares (PRESS) is another parameter to express the fitness of the model. The smaller the PRESS, the better the model fits the data points. In the present study, the calculated values of PRESS are 102.1, 42.945 and 160.032 for BG, MB and CV, respectively. The standard deviation and mean values were obtained to be less than 1.1 and larger than 89%, respectively. The following second order models were obtained after ANOVA study:

$$y_{MB} = 34.54 + 10.6X_1 + 1739X_2 + 4.4X_3 - 0.4X_4 - 0.444X_5 + 0.27X_6 + 213X_1X_2 + 0.5X_1X_3 - 0.3X_1X_4 - 0.3X_1X_5 + 133.4X_2X_4 + 54.8X_2X_5 - 29.3X_2X_6 + 0.23X_3X_4 + 0.4X_3X_5 - 0.103X_3X_6 - 0.15X_4X_5 + 0.23X_5X_6 - 0.96X_1^2 - 94378X_2^2 - 1.34X_3^2 - 0.11X_6^2 \quad (5)$$

$$y_{BG} = -70.4 + 14.6X_1 + 5042X_2 + 16.1X_3 + 6.8X_4 + 3.0X_5 - 1.3X_6 - 165.2X_1X_2 + 0.4X_1X_3 - 0.6X_1X_4 - 0.12X_1X_5 + 0.48X_1X_6 - 148X_2X_3 + 126.6X_2X_4 - 0.5X_3X_4 - 0.4X_3X_5 - 0.4X_3X_6 + 0.18X_4X_6 - 0.9X_1^2 - 92746X_2^2 - 0.84X_3^2 - 0.34X_4^2 - 0.18X_5^2 - 0.18X_6^2 \quad (6)$$

$$y_{CV} = 62.4 + -0.34X_1 + 1793X_2 + 10.6X_3 - 3.2X_4 + 5.8X_5 - 5.7X_6 + 130X_1X_2 + 0.26X_1X_4 - 0.4X_1X_5 + 0.5X_1X_6 + 113.4X_2X_4 - 48X_2X_5 + 87X_2X_6 + 0.21X_3X_4 + 0.3X_3X_6 - 0.25X_4X_5 - 0.22X_1^2 - 78905X_2^2 - 1.44X_3^2 - 0.1X_4^2 - 0.15X_6^2 \quad (7)$$

As mentioned above, Fig. 6a shows the good fit of the RSM model to the experimental data.

The analysis of the results is visualized using standardized main effect Pareto charts ( $P = 95\%$ ) and two factor interaction Pareto charts ( $P = 95\%$ ) as shown in Fig. 7. The results confirm that the factors of  $X_1$ ,  $X_2$ ,  $X_3$  and  $X_6$  as well as the quadratic effects of  $X_1^2$ ,  $X_2^2$  and  $X_3^2$  are the most effective factors.

#### 3.4. Response surface methodology

RSM is applied to optimize the parameters and explain the nature of the response surface in experiments. Fig. 8 shows the related fitted three dimensional response surfaces of  $R\%$  versus significant variables. These plots were achieved for a certain pair of variables at center values of other variables. Fig. 8a strongly supports that the MB removal percentage increases while increasing the pH and sonication time. It is worth to mention that the surface charge of  $\text{MnO}_2$ -NPs-AC at pHs lower than  $\text{pH}_{\text{ZPC}}$  is positive. At pH area higher than  $\text{pH}_{\text{ZPC}}$ , the adsorbent charge changes to negative and makes it possible to efficiently remove cationic compounds. According to above considerations, the basic conditions are more ideal for dyes adsorption. The maximum adsorption of dyes was achieved in middle sonication time. It was found that more than 95 % MB removal occurs in the 3.0 min and reaches equilibrium after about 4.0 min sonication. Fig. 8b shows behavior of  $R\%$  of MB versus the adsorbent and sonication time. The increase in the amount of adsorbent leads to significant decrease in sonication time, while at fixed amount of the adsorbent the removal percentage was observed to be increased with the increase in the sonication time. Fig. 8c shows the changes in the efficiency of BG removal using  $\text{MnO}_2$ -NP-AC. The BG concentration and initial pH of solution were varied while other four variables were held at zero level. A maximum removal efficiency of BG (99%) was reached when the initial pH of solution and BG concentration were 7 and 6  $\text{mg L}^{-1}$ , respectively. This result is due to the influence of pH of adsorption medium on the BG removal efficiency. As shown in Fig. 8d, the CV removal percentage varies as a function of adsorbent dosage with positive correlation, so that the adsorption increases with increase in adsorbent dosage (i.e. increase in specific surface area and reactive centers). Significant decrease in the removal percentage at lower amount of  $\text{MnO}_2$ -NP-AC is due to unbalancing the dye molecules to vacant sites ratio.

The effects of initial MB and BG dyes concentration on the removal percentages of MB and BG were shown in Figs. 8e and 8f, respectively. It was seen that the removal percentage of each dye

decreases by increasing the dyes concentration, which is due to the decrease in the ratio of available surface adsorption sites to the dyes molecules.

### 3.5. Optimization of dyes adsorption from aqueous solutions using RSM

After analyzing the polynomial equations modeling the dependent and independent variables, the process was further optimized and validated using desirability criterion of maximum removal of CV, BG and MB. A 3D plot helps to identify an optimum point on the response surface whereas a response optimizer allows setting a target for desired output and accordingly displays the optimum solution. The desirability profile for predicted values was obtained for the optimization of the process (Fig. 9). The desirability close to 1 indicates the most desired conditions and the corresponding responses. The RSM experiments were performed and the maximum R% of each dye was found to be higher than 99 %, while the minima of 62.55 %, 59.16 % and 58.32 % were observed for CV, BG and MB, respectively.

The optimized values, predicted from model presented in Fig. 9, were validated by running three experiments at similar condition as predicted, the results of which were in good agreement. Moreover, the adsorption studies also showed the highest efficiency for dyes removal where 0.022 g of the adsorbent was used during 4 min (sonication time) at pH 7 as well as where the initial concentration of each dye was set to be 6 mg L<sup>-1</sup> which was closer to optimized conditions predicted by the model. This confirms the suitability of the model for the prediction of process behavior.

### 3.6. Modeling by artificial neural network (ANN)

An ANN was used for modeling the adsorption studies based on the application of the experimental data at different operating conditions to train and test the neural network model.<sup>40</sup> The judgment on the efficiency of ANN model is based on the maximization of R<sup>2</sup> value and reduction of the MSE value of the training set (1–15 neurons correspond to hidden layer). Table 6 shows the relation among the number of neurons, R<sup>2</sup> and MSE for selected ANN model, while the R<sup>2</sup> and MSE values are larger than 0.9988 and less than 0.00085, respectively. Therefore, the ANN containing 8, 12 and 13 hidden neurons respectively for MB, BG and CV were selected as the best model for the prediction of adsorption behavior. The plot of predicted removal data for

the training and testing set (Fig. 6b) supports good agreement between the experimental and predicted data.

### 3.7. Application of adsorption models to equilibrium data

The adsorption isotherm describes the relationship between the amount of dye adsorbed at constant temperature and its concentration in the equilibrium solution. The isotherms are useful for estimating the total amount of adsorbent needed to adsorb a desired amount of adsorbate from solution.<sup>41</sup> In the present study equilibrium studies were carried out at 25°C. The equilibrium data were analyzed using three of the most commonly used isotherms, Langmuir, Freundlich, Temkin and Dubinin-radushkevich isotherm models at optimum condition.

The Eqs. 8-11 show the linear equations of the Langmuir,<sup>42</sup> Freundlich,<sup>43</sup> Temkin,<sup>44</sup> and Dubinin-radushkevich,<sup>45</sup> respectively:

$$\frac{C_e}{q_e} = \frac{1}{Q_m K_L} + \frac{C_e}{Q_m} \quad (8)$$

where  $Q_m$  is the maximum monolayer sorption capacity ( $mg\ g^{-1}$ ) and  $K_L$  is Langmuir constant related to the energy of adsorption ( $L\ mg^{-1}$ ).

$$\ln q_e = \ln K_F + \frac{1}{n} \ln C_e \quad (9)$$

where  $K_F$  ( $L\ g^{-1}$ ) and  $n$  (dimensionless) are Freundlich constants, being indicative of the adsorption capacity and adsorption intensity, respectively.

$$q_e = B \ln K_T + B \ln C_e \quad (10)$$

where  $B = RT/b$ ,  $T$  is the absolute temperature in  $K$ ,  $R$  the universal gas constant,  $8.314\ J\ mol^{-1}\ K^{-1}$ ,  $K_T$  the equilibrium binding constant ( $L\ mg^{-1}$ ) and  $b$  is related to the heat of adsorption.



$$\ln q_e = \ln Q_s - \beta \varepsilon^2 \quad (11)$$

where  $\varepsilon = RT \ln (1 + 1/C_e)$  (Polanyi potential),  $Q_s$  is the adsorption capacity ( $mg\ g^{-1}$ ),  $\beta$  is the constant related to the adsorption energy,  $R$  is the gas constant and  $T$  is the absolute temperature (K).

Using the activity coefficient, it is possible to estimate the mean energy of the adsorption ( $kJ\ mol^{-1}$ ) which represents an indication of the mechanism involved in the adsorption, according to Eq. (12):

$$E = \frac{1}{\sqrt{2\beta}} \quad (12)$$

The essential characteristics of Langmuir isotherm can be expressed by a dimensionless constant called equilibrium parameter as

$$R_L = \frac{I}{I + K_L C_0} \quad (13)$$

where  $K_L$  is the Langmuir constant, and  $C_0$  is the highest initial dye concentration ( $mg\ L^{-1}$ ). The value of  $R_L$  indicates the type of isotherm, i.e. either to be unfavorable ( $R_L > 1$ ), linear ( $R_L = 1$ ), favorable ( $0 < R_L < 1$ ), or irreversible ( $R_L = 0$ ). The  $R_L$  values obtained are in the range of 0-1 as shown in Table 7, thus indicating the favorable dyes adsorption onto  $MnO_2$ -NP-AC.

The Langmuir, Freundlich Temkin and Dubinin-radushkevich parameters were obtained at optimum condition according to the intercept and slope from the plots between  $C_e/q_e$  vs.  $C_e$  (Fig. 10a), and  $\ln q_e$  vs.  $\ln C_e$  (Fig. 10b),  $q_e$  vs.  $\ln C_e$  (Fig. 10c) and  $\ln q_e$  vs.  $\varepsilon^2$ , respectively.

The outcome values of parameters  $Q_m$ ,  $K_L$ ,  $K_F$ ,  $1/n$ ,  $B$ ,  $K_T$ ,  $Q_s$ ,  $\beta$ ,  $E$  and  $R^2$  for all the experiments for the removal of dyes are presented in Table 7.

The comparison of correlation coefficients ( $R^2$ ) of the linearized form of the three isotherm models indicates that the Langmuir model (see Fig. 10a) yields a better fit for the experimental equilibrium adsorption data than the Freundlich, Temkin and Dubinin-radushkevich isotherm models. The experimental data of three dyes produced a higher value of correlation coefficients (0.995) with Langmuir model than Freundlich (0.927-0.986), this behavior suggests the

monolayer coverage of the surface of adsorbent by dyes molecules.

The correlation coefficient ( $R^2$ ) and non-linear chi-square test ( $\chi^2$ ) were obtained and shown in Table 7. It was found that the smaller  $\chi^2$  and higher  $R^2$  values for the Langmuir isotherm amongst the applied models confirm the high efficiency of the Langmuir isotherm to represent the experimental data. In other words, the Langmuir isotherm is the most applicable model.

The results were also fitted by the Temkin model (see Table 7), which suggested a reduction in the heat of adsorption along with coverage due to sorbent-adsorbate interactions. As a result, adsorption of dyes could be characterized by a uniform distribution of binding energies up to maximum value.

The free energy of dyes adsorption was considered via Dubinin-radushkevich (D-R) model. As can be seen from Table 7, the experimental results were fitted by D-R model with a relatively good correlation coefficient (0.90-0.98). The values of the calculated mean energy ( $E$ ) of adsorption for all three dyes were less than  $8 \text{ kJ mol}^{-1}$ . The increase in  $E$  value with increasing the adsorbent mass shows higher tendency of dye molecule for the adsorption onto the adsorbent surface.

### 3.8. Kinetics

Several kinetic models are available in the literature to describe the mechanism of solute adsorption onto an adsorbent. In this work, the adsorption of the three selected dyes onto MnO<sub>2</sub>-NP-AC was investigated by the pseudo first-order,<sup>46</sup> pseudo second-order,<sup>47</sup> intraparticle diffusion,<sup>48</sup> and Elovich,<sup>49</sup> models to find most suitable one describing the kinetics of the adsorption process.

The linear form of the pseudo first-order rate expression of Lagergren<sup>46</sup> can be written as:

$$\log(q_e - q_t) = \log q_e - \left(\frac{k_1}{2.303}\right)t \quad (14)$$

where  $q_e$  and  $q_t$  are the specific amounts of dye adsorbed ( $\text{mg g}^{-1}$ ) at equilibrium and after a time  $t$  (min), respectively, and  $k_1$  is the pseudo-first-order rate constant ( $1.\text{min}^{-1}$ ). The  $\log (q_e - q_t)$  versus  $t$  was plotted (see Fig. 10d) and the values of  $k_1$  and  $q_e$  were determined by using the slope and intercept of the line, respectively.

The pseudo second-order model can be expressed in the following linear form:<sup>47</sup>

$$\frac{t}{q_t} = \frac{1}{k_2 q_e^2} + \frac{t}{q_e} \quad (15)$$

where  $k_2$  is the pseudo second-order rate constant ( $g \text{ mg}^{-1} \text{ min}^{-1}$ ). The values of  $k_2$  and  $q_t$  were estimated for the three dyes from the intercepts and slopes of straight lines obtained from the plot of  $t/q_t$  versus  $t$  (see Fig. 10e).

The intraparticle diffusion equation is given as:<sup>48</sup>

$$q_t = K_{dif} t^{1/2} + C \quad (16)$$

where  $K_{dif}$  is the intraparticle diffusion rate constant ( $mg \text{ (g.min}^{1/2})^{-1}$ ) and  $C$  shows the boundary layer thickness. The values of  $K_{dif}$  (the intraparticle diffusion rate constant ( $mg \text{ g}^{-1} \text{ min}^{-1/2}$ )) and  $C$  (an indication of the thickness of the boundary layer) were calculated from the slope and intercept of the plot of  $q_t$  versus  $t^{1/2}$ .

The Elovich kinetic model<sup>49</sup> is described by Eq. (17):

$$q_t = \frac{1}{\beta} \ln(\alpha\beta) + \frac{1}{\beta} \ln t \quad (17)$$

where  $\beta$  is the initial sorption rate due to  $dq/dt$  with  $q_t = 0$  ( $mg \text{ g}^{-1} \text{ min}^{-1}$ ) and  $\alpha$  is the desorption constant of the Elovich model ( $g \text{ mg}^{-1}$ ). The plot of  $q_t$  versus  $\ln(t)$  should yield a linear relationship with a slope of  $(1/\beta)$  and an intercept of  $(1/\beta) \ln(\alpha\beta)$  if the Elovich is applicable (see Fig. 10f).

Table 8 lists the values of the rate constants of the four kinetic models tested in this study, namely the pseudo first-order, pseudo second-order, intraparticle diffusion and Elovich models, along with their respective  $R^2$  and  $\chi^2$  values that were estimated by linear fitting of experimental data collected at various times.

The correlation coefficient ( $R^2$ ) values for the pseudo-second order rate equation (0.996–0.999 for CV, 0.999 for BG and 0.999 for MB) were found to be higher than those for pseudo-first order rate equation (0.960-0.977 for CV, 0.818-0.977 for BG and 0.876-0.977 for MB). The  $q_e(\text{exp})$  values (48.90-145.26 mg g<sup>-1</sup> for CV; 47.22-133.40 mg g<sup>-1</sup> for BG and 49.32-139-10 mg g<sup>-1</sup> for MB) were in close agreement with  $q_e(\text{calc})$  (51.28-149.25 mg g<sup>-1</sup> for CV; 48.544-135.14 mg g<sup>-1</sup> for BG and 50.08-140.85 mg g<sup>-1</sup> for MB) for pseudo-second order model.

It was seen that the intraparticle diffusion model was inappropriate to describe adsorption kinetics while the Elovich model was the best to represent the adsorption of dyes onto MnO<sub>2</sub>-NP-AC ( $R^2 = 0.920$ - $0.992$ ). The pseudo second-order model exhibited the best fit ( $R^2 > 0.995$  for all sets of runs).

### 3.9. Comparison of RSM and ANN

The judgment on the usefulness of ANN and RSM models is based on the criteria such as the absolute average deviation (AAD), mean squared error (RMS), mean absolute error (MAE) and the correlation coefficient ( $R^2$ ) calculated by Eqs. (18-21), respectively.<sup>50</sup>

$$\text{AAD}\% = \left( \frac{1}{n} \sum_{i=1}^n \left( \frac{y_{i,\text{pred}} - y_{i,\text{exp}}}{y_{i,\text{pred}}} \right) \right) \times 100 \quad (18)$$

$$\text{RMS} = \sqrt{\frac{\sum_{i=1}^n (y_{i,\text{pred}} - y_{i,\text{exp}})^2}{n}} \quad (19)$$

$$\text{MAE} = \frac{\sum_{i=1}^n |y_{i,\text{pred}} - y_{i,\text{exp}}|}{n} \quad (20)$$

$$R^2 = 1 - \sum_{i=1}^n \left( \frac{(y_{i,\text{pred}} - y_{i,\text{exp}})^2}{(y_{\text{avg,exp}} - y_{i,\text{exp}})^2} \right) \quad (21)$$

where  $n$  is the number of experimental data ( $n=10$  in Table 9),  $y_{i,\text{pred}}$  and  $y_{i,\text{exp}}$  are the predicted and experimental responses, respectively, and  $y_{\text{avg,exp}}$  is the average of experimental values.  $R^2$  is a measure of the amount of the reduction in the variability of the response by using the repressor variables in the model while AAD is a direct method for describing deviations.  $R^2$  must be

closed to 1.0 and the AAD between predicted and experimental data must be as small as possible.<sup>51</sup> ANN and RSM were compared in terms of R, R<sup>2</sup>, AAD, RMS and MAE performance parameters.

Table 9 shows the observed and modeled results of six test experiments at optimum conditions and ten test experiments for unseen data. This table suggested that ANN model is not only stable and flexible, but also offer a certain degree of extrapolation outside the training data. The RSM was also applied well. However, the ANN showed an overall better applicability than the RSM.

Fig. 6 indicates the comparative plot for RSM and ANN prediction for the designed experiments. The generalization capability can be best judged only with completely unseen dataset. Therefore, it was decided to test both the models using unseen data. The experimental and predicted removal percentages are summarized in Table 9. The correlation coefficients for unseen data by ANN were obtained to be 0.9991, 0.9978 and 0.9969 for MB, BG and CV, respectively, while the corresponding values for RSM were found to be 0.9975, 0.9968 and 0.9964. The comparative values of correlation coefficient, AAD, MAE and RMS are given in Table 9. The values of AAD for RSM were obtained to be 0.4162 for MB, 0.5909 for BG and 0.7601 for CV. The AAD for ANN were found to be 0.4518 for MB, 0.4518 for BG and 0.6202 for CV. The Absolute errors for ANN and RSM models were > 2 % and < 2 %, respectively, for all dyes. The MAE and RMS for ANN model are Lower than RSM model. It was found that both models are applicable to predict the experimental data. However, the prediction capability of ANN model was higher than the RSM model. This upper predictive accuracy of ANN model can be attributed to its universal capability to approximate non-linearity of the system, while RSM is only restricted to second-order polynomial.

### 3.10. Comparison of the presented procedure with other methods

Table 10 compares the pH, adsorption capacity ( $mg\ g^{-1}$ ) and contact time (min) of the different types of adsorbents used for the removal of dyes. The value of ( $Q_{max}$ ) in this study using an environmental friendly and low cost adsorbent is significantly higher than those in most of the previous works.<sup>6, 8, 10-13, 19, 52-71</sup> As seen in Table 10, the contact time for the proposed method is preferable and superior to the literature. This may be associated with the homogeneous surface of the MnO<sub>2</sub>-NP-AC. The rapid uptake and quick establishment of equilibrium show the efficiency of ultrasound power in wastewater treatment. Ultrasound is a highly recommended tool to

improve the mass transfer process and the affinity between adsorbate and adsorbent. The other advantage of this process is its neutral working pH.

#### 4. Conclusion

The rapid and simultaneous ultrasound-assisted adsorption of CV, BG and MB from aqueous solution and the effects of parameters on the adsorption in the batch system were successfully modeled using RSM and ANN where the MnO<sub>2</sub>-NP-AC was used as an efficient, environmental friendly and cost-effective adsorbent. The most important conclusions from this work are summarized as follows:

- 1) The optimum conditions were found as initial pH of 7.0, sonication time of 4.0 min, initial dyes concentration of 6 mg L<sup>-1</sup>, adsorbent dosage of 0.022 g. A small amount of the adsorbent (0.04 g) was capable to remove high percentage of dyes, i.e. 97, 100 and 100 % for CV, BG and MB, respectively.
- 2) The results of RSM and ANN methodologies based on validation data showed that RSM ( $R^2 > 0.987$ ) and ANN ( $R^2 > 0.990$ ) are useful and accurate methods to predict adsorption process.
- 3) The experimental equilibrium data fitting to Langmuir, Freundlich, Temkin and Dubinin–Radushkevich models showed that the Langmuir model applies well for the evaluation and description of the actual behavior of adsorption with high adsorption capacity in single component system (263.16, 206.2 and 234.20 mg g<sup>-1</sup> for CV, BG and MB, respectively).
- 4) The pseudo-second-order rate model accurately described the kinetics of the adsorption.
- 5) MnO<sub>2</sub>-NP-AC has high adsorption capacity compared to other adsorbents for dyes removal from aqueous medium.

#### Acknowledgement

The authors express their appreciation to the Graduate School and Research Council of the Yasouj University for their financial support.

**References:**

1. R. Wangpradit and P. Chitprasert, *Int. Biodeterior. Biodegrad.*, 2014, **93**, 168-176.
2. E. Forgacs, T. Cserhati and G. Oros, *Environ. Int.*, 2004, **30**, 953-971.
3. M. Ghaedi, A. Ghaedi, F. Abdi, M. Roosta, A. Vafaei and A. Asghari, *Ecotoxicol. Environ. Saf.*, 2013, **96**, 110-117.
4. S. Hajati, M. Ghaedi and H. Mazaheri (2014): *Desalination and Water Treatment*, DOI: 10.1080/19443994.2014.981217.
5. M. Ghaedi, H. Hossainian, M. Montazerozohori, A. Shokrollahi, F. Shojaipour, M. Soylak and M. K. Purkait, *Desalination*, 2011, **281**, 226-233.

6. A. Saeed, M. Sharif and M. Iqbal, *J. Hazard. Mater.*, 2010, **179**, 564-572.
7. Y. Lin, X. He, G. Han, Q. Tian and W. Hu, *J. Environ. Sci.*, 2011, **23**, 2055-2062.
8. N. Zeinali, M. Ghaedi and G. Shafie, *J. Ind. Eng. Chem.*, 2014, **20**, 3550-3558.
9. A. Asfaram, M. Ghaedi, S. Agarwal, I. Tyagi and V. Kumar Gupta, *RSC Adv.*, 2015, **5**, 18438-18450.
10. M. Ghaedi, N. Zeinali, A. M. Ghaedi, M. Teimuori and J. Tashkhourian, *Spectrochim. Acta, Part A*, 2014, **125**, 264-277.
11. X. Zhang, P. Zhang, Z. Wu, L. Zhang, G. Zeng and C. Zhou, *Colloids Surf. A Physicochem Eng. Asp.*, 2013, **435**, 85-90.
12. M. Ghaedi, A. Ghaedi, M. Hossainpour, A. Ansari, M. Habibi and A. Asghari, *J. Ind. Eng. Chem.*, 2014, **20**, 1641-1649.
13. M. K. Satapathy and P. Das, *J. Environ. Chem. Eng.*, 2014, **2**, 708-714.
14. D. Morshedi, Z. Mohammadi, M. M. A. Boojar and F. Aliakbari, *Colloids Surf. B*, 2013, **112**, 245-254.
15. Z. Yang, H. Yang, Z. Jiang, T. Cai, H. Li, H. Li, A. Li and R. Cheng, *J. Hazard. Mater.*, 2013, **254**, 36-45.
16. F. Gulshan, S. Yanagida, Y. Kameshima, T. Isobe, A. Nakajima and K. Okada, *Water Res.*, 2010, **44**, 2876-2884.
17. S. Raghu, C. W. Lee, S. Chellammal, S. Palanichamy and C. A. Basha, *J. Hazard. Mater.*, 2009, **171**, 748-754.
18. M. Bagheri, H. Younesi, S. Hajati, S. M. Borghei, *Int. J. Bio. Macromolecules*, 2015, **80**, 431-444.
19. S. Hajati, M. Ghaedi, B. Barazesh, F. Karimi, R. Sahraei, A. Daneshfar and A. Asghari, *J. Ind. Eng. Chem.*, 2014, **20**, 2421-2427.
20. F. Nasiri azad, M. Ghaedi, K. Dashtian, M. Montazerzohori, S. Hajati and E. Alipanahpour, *RSC Adv.*, 2015, **5**, 61060-61069.
21. M. Roosta, M. Ghaedi, A. Daneshfar, R. Sahraei and A. Asghari, *J. Ind. Eng. Chem.*, 2015, **21**, 459-469.
22. A.R. Bagheri, M. Ghaedi, S. Hajati, A.M. Ghaedi, A. Goudarzi and A. Asfaram, *RSC Adv.*, 2015, **5**, 59335-59343.



23. M. Ghaedi, A. Ansari, F. Bahari, A. M. Ghaedi and A. Vafaei, *Spectrochim. Acta, Part A*, 2015, **137**, 1004-1015.
24. M. Khajeh, M. Kaykhahi and A. Sharafi, *J. Ind. Eng. Chem.*, 2013, **19**, 1624-1630.
25. S. Hajati, S. Tougaard, J. Walton and N. Fairley, *Surf. Sci.*, 2008, **602**, 3064-3070.
26. J. Zolgharnein and A. Shahmoradi, *J. Chem. Eng. Data*, 2010, **55**, 3428-3437.
27. M. Maghsoudi, M. Ghaedi, A. Zinali, A. M. Ghaedi and M. H. Habibi, *Spectrochim. Acta, Part A*, 2015, **134**, 1-9.
28. M. Ghaedi, E. Alam Barakat, A. Asfaram, B. Mirtamizdoust, A.A. Bazrafshan and S. Hajati, *RSC Adv.*, 2015, **5**, 42376-42387.
29. M. Jamshidi, M. Ghaedi, K. Dashtian, S. Hajati and A.A. Bazrafshan, *RSC Adv.*, 2015, **5**, 59522-59532.
30. M. Ghaedi, S.Y.S. Jaber, S. Hajati, M. Montazerzohori, A. Asfaram and M. Zare, *IEEE Sensors Journal*, 2015, **15**, 2974-2983.
31. S. Hajati, M. Ghaedi and S. Yaghoubi, *J. Ind. Eng. Chem.*, 2015, **21**, 760-767.
32. M. Ghaedi, H. Mazaheri, S. Khodadoust, S. Hajati and M.K. Purkait, *Spectrochimica Acta A*, 2015, **135**, 479-490.
33. A. Asfaram, M. Ghaedi, S. Hajati, A. Goudarzi and A. A. Bazrafshan, *Spectrochim. Acta, A*, 2015, **145**, 203-212.
34. M. Ghaedi, S. Hajati, M. Zare, M. Zare and S.Y. Shajaripour Jaber, *RSC Adv.*, 2015, **5**, 38939-38947.
35. S. Hajati, M. Ghaedi, Z. Mahmoudi and R. Sahraei, *Spectrochimica Acta A*, 2015, **150**, 1002-1012.
36. X. Chu and H. Zhang, *Modern Appl. Sci.*, 2009, **3**, P177.
37. D. Jaganyi, M. Altaf and I. Wekesa, *Appl. Nanosci.*, 2013, **3**, 329-333.
38. Y. C. Zhang, T. Qiao, X. Y. Hu and W. D. Zhou, *J. Cryst. Growth*, 2005, **280**, 652-657.
39. X. Guan and H. Yao, *Food Chem.*, 2008, **106**, 345-351.
40. S. Elemen, E. P. A. Kumbasar and S. Yapar, *Dye. Pigm.*, 2012, **95**, 102-111.

41. R. Jain and M. Shrivastava, *J. Hazard. Mater.*, 2008, **152**, 216-220.
42. I. Langmuir, *J. Am. Chem. Soc.*, 1916, **38**, 2221-2295.
43. H. Freundlich, *Z Phys. Chem.*, 1906, **57**, 385-471.
44. M. Temkin and V. Pyzhev, *Acta physiochim. URSS*, 1940, **12**, 217-222.
45. M. Dubinin and L. Radushkevich, *Chem. Zentr*, 1947, **1**, 875-889.
46. S. Lagergren, *K. Sven. vetensk.akad. handl.*, 1898, **24**, 1-39.
47. Y.-S. Ho and G. McKay, *Process Biochem.*, 1999, **34**, 451-465.
48. E. Daneshvar, M. Kousha, M. S. Sohrabi, A. Khataee and A. Converti, *Chem. Eng. J.*, 2012, **195**, 297-306.
49. C. A. Başar, *J. Hazard. Mater.*, 2006, **135**, 232-241.
50. M. Antonopoulou, V. Papadopoulos and I. Konstantinou, *J. Chem. Technol. Biotechnol.*, 2012, **87**, 1385-1395.
51. E. Betiku and A. E. Taiwo, *Renew. Energ.*, 2015, **74**, 87-94.
52. R. Ahmad, *J. Hazard. Mater.*, 2009, **171**, 767-773.
53. C. Kannan, N. Buvaneswari and T. Palvannan, *J. Hazard. Mater.*, 2009, **249**, 1132-1138.
54. X. S. Wang, X. Liu, L. Wen, Y. Zhou, Y. Jiang and Z. Li, *Sep. Sci. Technol.*, 2008, **43**, 3712-3731.
55. R. Gong, S. Zhu, D. Zhang, J. Chen, S. Ni and R. Guan, *Desalination*, 2008, **230**, 220-228.
56. R. Kumar and R. Ahmad, *Desalination*, 2011, **265**, 112-118.
57. G. O. El-Sayed, *Desalination*, 2011, **272**, 225-232.
58. K. P. Singh, S. Gupta, A. K. Singh and S. Sinha, *J. Hazard. Mater.*, 2011, **186**, 1462-1473.
59. S. An, X. Liu, L. Yang and L. Zhang, *Chem. Eng. Res. Des.*, 2015, **94**, 726-735.
60. M. Ghaedi, G. Negintaji, H. karimi and F. Marahel, *J. Ind. Eng. Chem.*, 2014, **20**, 1444-1452.
61. T. Calvete, E. C. Lima, N. F. Cardoso, S. L. Dias and E. S. Ribeiro, *Clean-Soil, Air, Water*, 2010, **38**, 521-532.

62. J. Zolgharnein, M. Bagtash and T. Shariatmanesh, *Spectrochim. Acta, Part A*, 2015, **137**, 1016-1028.
63. R. Kumar, M. O. Ansari and M. Barakat, *Ind. Eng. Chem. Res.*, 2014, **53**, 7167-7175.
64. S. Qu, F. Huang, S. Yu, G. Chen and J. Kong, *J. Hazard. Mater.*, 2008, **160**, 643-647.
65. J. Yang and K. Qiu, *Chem. Eng. J.*, 2010, **165**, 209-217.
66. M. Ghaedi, S. Heidarpour, S. Nasiri Kokhdan, R. Sahraie, A. Daneshfar and B. Brazesh, *Powder Technol.*, 2012, **228**, 18-25.
67. M. Roosta, M. Ghaedi, A. Daneshfar, R. Sahraei and A. Asghari, *Ultrason. Sonochem.*, 2014, **21**, 242-252.
68. T. Liu, Y. Li, Q. Du, J. Sun, Y. Jiao, G. Yang, Z. Wang, Y. Xia, W. Zhang and K. Wang, *Colloids Surf., B*, 2012, **90**, 197-203.
69. J. Fu, Z. Chen, M. Wang, S. Liu, J. Zhang, J. Zhang, R. Han and Q. Xu, *Chem. Eng. J.*, 2015, **259**, 53-61.
70. M. Ghaedi, S. Hajjati, Z. Mahmudi, I. Tyagi, S. Agarwal, A. Maity and V. Gupta, *Chem. Eng. J.*, 2015, **268**, 28-37.
71. M. Ghaedi, M. Pakniat, Z. Mahmoudi, S. Hajati, R. Sahraei and A. Daneshfar, *Spectrochim. Acta, Part A*, 2014, **123**, 402-409.

**Table 1.** Derivative equations for the dyes.

derivative	dye	$\lambda$ (nm)	Regression equation	R <sup>2</sup>
First order derivative	BG	392	$dA/d\lambda = 4.22084 \times 10^{-4}C + 2.15655 \times 10^{-4}$	0.989313
Second order derivative	MB	710	$d^2A/d^2\lambda = 5.6846 \times 10^{-5}C + 8.73000 \times 10^{-8}$	0.996044
	BG	440	$d^3A/d^3\lambda = 7.31540 \times 10^{-6}C + 1.78820 \times 10^{-6}$	0.999416
Third order derivative	CV	550	$d^3A/d^3\lambda = 5.17230 \times 10^{-6}C + 5.00300 \times 10^{-7}$	0.998993
	MB	710	$d^3A/d^3\lambda = -6.96820 \times 10^{-5}C - 2.13090 \times 10^{-6}$	0.999277

Fourth order derivative	BG	428	$d^4A/d^4\lambda = 7.54900 \times 10^{-5}C + 5.16300 \times 10^{-7}$	0.992576
	CV	543	$d^4A/d^4\lambda = 2.34400 \times 10^{-7}C + 3.74000 \times 10^{-7}$	0.994429
	MB	714	$d^4A/d^4\lambda = 6.18200 \times 10^{-7}C + 7.50000 \times 10^{-7}$	0.998220

**Table 2.** Experimental factors and levels in the central composite design.

Factors	Levels			$\alpha = 2.82843$	
	Low (-1)	Central (0)	High (+1)	$-\alpha$	$+\alpha$
X <sub>1</sub> :pH	6	7	8	4.171573	9.828427
X <sub>2</sub> : Adsorbent dosage (g)	0.01	0.015	0.02	0.000858	0.029142
X <sub>3</sub> : Sonication time (min)	3	4	5	1.171573	6.828427
X <sub>4</sub> : MB concentration (mg L <sup>-1</sup> )	4	6	8	0.343146	11.65675
X <sub>5</sub> : BG concentration (mg L <sup>-1</sup> )	4	6	8	0.343146	11.65675
X <sub>6</sub> : CV concentration (mg L <sup>-1</sup> )	4	6	8	0.343146	11.65675



**Table 3.** Experimental conditions and values obtained through the CCD.

Run	X <sub>1</sub>	X <sub>2</sub>	X <sub>3</sub>	X <sub>4</sub>	X <sub>5</sub>	X <sub>6</sub>	%R <sub>MB</sub>	%R <sub>BG</sub>	%R <sub>CV</sub>	Run	X <sub>1</sub>	X <sub>2</sub>	X <sub>3</sub>	X <sub>4</sub>	X <sub>5</sub>	X <sub>6</sub>	%R <sub>MB</sub>	%R <sub>BG</sub>	%R <sub>CV</sub>
1	0	0	0	0	0	0	96.8	97.3	93.2	46	0	0	+ $\alpha$	0	0	0	87.2	95.4	86.8
2	0	0	0	0	0	0	95.8	95.3	94.0	47	+1	-1	+1	+1	-1	+1	79.1	80.9	83.8
3	-1	+1	-1	+1	+1	+1	97.5	100.0	84.1	48	0	0	0	0	0	0	95.6	96.7	95.3
4	-1	-1	+1	-1	+1	-1	88.8	87.6	95.5	49	-1	+1	+1	+1	-1	-1	98.1	98.1	96.2
5	-1	+1	+1	+1	-1	+1	95.2	95.1	92.5	50	+1	+1	-1	-1	+1	+1	97.1	96.9	92.1
6	+1	+1	+1	+1	-1	+1	95.6	95.5	100.2	51	-1	-1	-1	+1	-1	+1	83.9	76.9	71.7
7	-1	+1	-1	-1	-1	-1	98.1	90.9	95.6	52	+1	+1	+1	+1	-1	-1	98.8	95.6	100.0
8	+ $\alpha$	0	0	0	0	0	85.9	92.8	95.1	53	-1	+1	+1	+1	+1	+1	99.1	97.9	89.3
9	+1	-1	-1	+1	+1	-1	72.2	79.8	80.2	54	+1	-1	-1	+1	-1	+1	77.6	78.6	75.2
10	+1	+1	+1	-1	+1	-1	100.1	100.0	99.5	55	-1	-1	+1	+1	+1	+1	83.8	81.2	76.3
11	-1	+1	-1	+1	-1	-1	97.5	95.4	93.5	56	-1	-1	-1	+1	+1	+1	82.2	81.6	70.9
12	+1	-1	-1	-1	+1	-1	82.2	85.3	89.5	57	+1	+1	-1	-1	-1	-1	100.1	90.6	97.5
13	0	0	0	0	0	+ $\alpha$	91.5	90.8	82.1	58	+1	+1	+1	+1	+1	+1	97.2	99.9	93.9
14	-1	-1	-1	+1	+1	-1	80.2	80.1	82.9	59	0	0	0	0	0	0	96.3	96.0	95.7
15	+1	+1	+1	-1	-1	+1	94.2	97.8	97.4	60	+1	+1	-1	-1	-1	+1	95.3	92.1	94.2
16	0	0	0	0	0	0	95.7	96.0	92.3	61	-1	-1	-1	-1	+1	-1	87.4	80.6	92.4
17	-1	-1	+1	-1	-1	-1	87.7	86.5	89.7	62	-1	-1	-1	+1	-1	-1	84.5	75.7	81.0
18	0	0	0	0	0	0	96.5	94.8	95.0	63	+1	+1	-1	+1	+1	-1	93.2	96.5	92.8
19	0	0	0	0	0	0	95.8	95.4	93.8	64	+1	-1	-1	+1	-1	-1	78.5	74.2	82.1
20	-1	-1	+1	-1	-1	+1	83.9	80.0	81.2	65	+1	-1	+1	+1	+1	+1	78.5	86.0	79.8
21	+1	-1	+1	-1	-1	+1	83.1	89.0	85.0	66	- $\alpha$	0	0	0	0	0	91.5	86.8	90.6
22	-1	+1	+1	-1	+1	+1	98.7	94.2	93.5	67	0	0	0	0	0	0	96.0	97.5	93.3
23	+1	+1	-1	+1	-1	-1	97.1	89.5	97.2	68	-1	-1	+1	+1	-1	+1	82.4	78.8	77.8
24	-1	+1	+1	+1	+1	-1	97.6	99.9	93.3	69	-1	+1	-1	-1	-1	+1	94.4	88.1	88.4
25	0	+ $\alpha$	0	0	0	0	96.6	97.4	95.1	70	-1	+1	+1	-1	-1	-1	96.6	97.0	96.5
26	0	0	0	0	0	0	96.4	97.0	93.2	71	0	0	0	0	- $\alpha$	0	94.9	85.6	94.0
27	-1	+1	-1	-1	+1	+1	97.9	94.6	92.3	72	+1	+1	+1	-1	+1	+1	99.3	100.3	96.5
28	0	0	0	0	0	0	95.8	95.9	95.0	73	-1	+1	+1	-1	-1	+1	91.6	92.2	92.0
29	+1	-1	+1	+1	+1	-1	77.7	84.2	82.5	74	+1	-1	-1	-1	-1	-1	86.8	79.5	87.4
30	+1	-1	+1	+1	-1	-1	81.8	80.5	85.3	75	+1	+1	-1	+1	+1	+1	93.6	101.2	89.7
31	-1	-1	+1	+1	-1	-1	83.5	82.5	84.2	76	-1	+1	0	-1	+1	-1	97.5	95.2	97.4
32	0	0	0	0	0	0	95.0	96.6	92.7	77	0	0	0	0	0	0	96.0	97.1	94.9
33	0	0	0	0	0	0	96.6	96.0	93.2	78	-1	+1	+1	-1	+1	-1	99.1	98.4	98.9
34	+1	-1	-1	-1	-1	+1	85.0	80.4	82.1	79	0	0	0	0	0	0	95.5	96.9	93.9
35	-1	+1	-1	+1	-1	+1	95.8	95.7	87.4	80	0	0	- $\alpha$	0	0	0	84.2	84.9	79.5
36	0	0	0	0	0	- $\alpha$	94.5	91.5	97.4	81	+1	+1	-1	+1	-1	+1	94.5	94.1	95.8
37	-1	-1	+1	-1	+1	+1	88.8	82.1	84.5	82	+1	+1	-1	-1	+1	-1	97.3	96.0	97.3
38	-1	-1	-1	-1	-1	-1	90.5	76.0	88.9	83	+1	-1	-1	-1	+1	+1	83.2	86.8	81.9
39	0	0	0	+ $\alpha$	0	0	88.8	85.4	85.3	84	+1	-1	+1	-1	+1	-1	85.3	91.8	88.2
40	+1	-1	+1	-1	+1	+1	86.3	91.7	85.3	85	+1	-1	+1	-1	-1	-1	86.1	93.4	91.0
41	0	0	0	0	+ $\alpha$	0	94.5	96.8	92.3	86	0	0	0	- $\alpha$	0	0	98.4	87.5	97.6
42	+1	+1	+1	-1	-1	-1	99.5	98.9	98.8	87	-1	-1	+1	+1	+1	-1	82.4	83.7	84.2
43	+1	-1	-1	+1	+1	+1	74.5	84.7	74.5	88	-1	-1	-1	-1	+1	+1	88.6	77.4	80.2
44	-1	+1	-1	+1	+1	-1	95.6	100.0	90.9	89	0	- $\alpha$	0	0	0	0	58.3	59.2	62.6
45	+1	+1	+1	+1	+1	-1	97.4	97.3	95.5	90	-1	-1	-1	-1	-1	+1	87.2	73.8	77.6

**Table 4.** Model summary statistics and Quality of quadratic model based on  $R^2$  and standard deviation for the adsorption of dyes onto  $MnO_2$ -NP-AC.

Model Summary Statistics															
Source	$R^2_{BG}$					$R^2_{MB}$					$R^2_{CV}$				
	SD <sup>a</sup>	$R^2$ <sup>b</sup>	Adjust <sup>c</sup>	Predict <sup>d</sup>	PRESS <sup>e</sup>	SD	$R^2$	Adjust	Predict	PRESS	SD	$R^2$	Adjust	Predict	PRESS
Linear	4.21	0.754	0.736	0.718	1690.3	3.96	0.759	0.741	0.717	1522.8	3.704	0.775	0.759	0.737	1335
2FI	3.72	0.84	0.795	0.812	1128.1	3.63	0.834	0.783	0.799	1081.53	3.303	0.854	0.809	0.817	94
Quadratic	0.83	0.993	0.990	0.983	102.1	0.53	0.997	0.995	0.992	42.945	1.03	0.987	0.981	0.969	160
Cubic	0.85	0.996	0.989	0.659	2042.4	0.52	0.998	0.996	0.814	999.765	1.15	0.991	0.977	0.358	3256
Quality of quadratic model based on $R^2$ and standard deviation															
Response	SD					Mean					CV% <sup>f</sup>				
$R^2_{BG}$	0.830					90.1					0.929				
$R^2_{MB}$	0.529					90.8					0.582				
$R^2_{CV}$	1.030					89.4					1.15				

<sup>a</sup> Standard deviation: square root of the pure (experimental) error.

<sup>b</sup> Coefficient of determination.

<sup>c</sup> Adjusted coefficient of determination.

<sup>d</sup> Predicted coefficient of determination.

<sup>e</sup> Predicted Residual Sum of Squares: a measure of how this particular model fits each point in the design.

<sup>f</sup> Coefficient of variation, the standard deviation as a percentage of mean.

<sup>g</sup> Adequate precision: compares the range of predicted values at design points to the average prediction error.

**Table 5.** Analysis of variance (ANOVA) for the adsorption of dyes onto MnO<sub>2</sub>-NP-AC

Source of variation	Df <sup>b</sup>	CV				BG				MB			
		SS <sup>a</sup>	MS <sup>c</sup>	F-value	P-value	SS <sup>a</sup>	MS <sup>c</sup>	F-value	P-value	SS <sup>a</sup>	MS <sup>c</sup>	F-value	P-value
Model	27	5370	199	711	< 0.0001	5950	220	322	< 0.0001	5010	185	175	< 0.0001
X <sub>1</sub>	1	88.21	88.21	81.214	0.0000	98.1	98.1	147.12	0.0000	87.25	87.25	365.53	0.0000
X <sub>1</sub> <sup>2</sup>	1	5.70	5.7	5.226	0.0397	91.04	91.04	136.6	0.0000	108.1	108.1	452.87	0.0000
X <sub>2</sub>	1	2632	2632	2423.3	0.0000	3802.4	3802.4	5703.5	0.0000	3715	3715	15564	0.0000
X <sub>2</sub> <sup>2</sup>	1	459.8	459.8	423.32	0.0000	635.21	635.21	952.8	0.0000	657.8	657.8	2755.6	0.0000
X <sub>3</sub>	1	192.5	192.5	177.2	0.0000	318.16	318.16	477.24	0.0000	19.5	19.5	81.67	0.0000
X <sub>3</sub> <sup>2</sup>	1	245.0	245.0	225.6	0.0000	82.778	82.778	124.2	0.0000	210.7	210.7	882.53	0.0000
X <sub>4</sub>	1	397.2	397.2	365.7	0.0000	11.026	11.026	16.538	0.0013	238.3	238.3	998.41	0.0000
X <sub>4</sub> <sup>2</sup>	1	19.12	19.12	17.607	0.0011	199.4	199.4	299.1	0.0000	14.02	14.02	58.75	0.0000
X <sub>5</sub>	1	8.418	8.418	7.751	0.0155	285.12	285.12	427.67	0.0000	0.256	0.256	1.07	0.3196
X <sub>5</sub> <sup>2</sup>	1	4.090	4.090	3.766	0.0743	59.753	59.753	89.629	0.0000	5.052	5.052	21.16	0.0005
X <sub>6</sub>	1	615.2	615.2	566.39	0.0000	3.773	3.773	5.659	0.0334	22.43	22.43	93.95	0.0000
X <sub>6</sub> <sup>2</sup>	1	43.4	43.4	39.933	0.0002	59.617	59.617	89.424	0.0000	20.83	20.83	87.27	0.0000
X <sub>1</sub> X <sub>2</sub>	1	26.9	26.9	24.730	0.0003	43.664	43.664	65.495	0.0000	72.4	72.4	303.07	0.0000
X <sub>1</sub> X <sub>3</sub>	1	0.118	0.118	0.109	0.7466	8.661	8.661	12.991	0.0032	17.52	17.52	73.39	0.0000
X <sub>1</sub> X <sub>4</sub>	1	16.8	16.8	15.463	0.0020	100.13	100.13	150.2	0.0000	20.6	20.69	86.08	0.0000
X <sub>1</sub> X <sub>5</sub>	1	33.8	33.8	31.102	0.0001	3.933	3.933	5.899	0.0304	16.79	16.79	70.36	0.0000
X <sub>1</sub> X <sub>6</sub>	1	63.4	63.4	58.387	0.0000	57.458	57.458	86.186	0.0000	0.562	0.562	2.36	0.1488
X <sub>2</sub> X <sub>3</sub>	1	1.011	1.011	0.931	0.3522	35.193	35.193	52.789	0.0000	0.018	0.018	0.08	0.7852
X <sub>2</sub> X <sub>4</sub>	1	82.31	82.31	75.786	0.0000	102.51	102.51	153.76	0.0000	113.9	113.9	477.04	0.0000
X <sub>2</sub> X <sub>5</sub>	1	14.7	14.7	13.527	0.0028	0.215	0.215	0.323	0.5796	19.22	19.22	80.50	0.0000
X <sub>2</sub> X <sub>6</sub>	1	48.4	48.4	44.560	0.0001	0.985	0.985	1.477	0.2458	5.495	5.495	23.02	0.0004
X <sub>3</sub> X <sub>4</sub>	1	10.9	10.9	10.015	0.0075	62.713	62.713	94.068	0.0000	13.22	13.22	55.39	0.0000
X <sub>3</sub> X <sub>5</sub>	1	1.2	1.2	1.094	0.3150	40.563	40.563	60.843	0.0000	38.49	38.49	161.25	0.0000
X <sub>3</sub> X <sub>6</sub>	1	22.42	22.42	20.641	0.0006	39.688	39.688	59.532	0.0000	2.698	2.698	11.30	0.0051
X <sub>4</sub> X <sub>5</sub>	1	65.33	65.33	60.149	0.0000	3.181	3.181	4.772	0.0478	23.67	23.7	99.07	0.0000
X <sub>4</sub> X <sub>6</sub>	1	6.9	6.9	6.336	0.0258	31.856	31.856	47.784	0.0000	8.124	8.124	34.03	0.0001
X <sub>5</sub> X <sub>6</sub>	1	2.83	2.83	2.606	0.1305	3.644	3.644	5.466	0.0360	53.21	53.21	222.92	0.0000
Lack-of-Fit	49	51.52	1.051	0.968	0.5631	33.820	0.690	1.035	0.5033	14.22	0.290	1.22	0.3652
Pure Error	13	14.12	1.086			8.667	0.667			3.103	0.239		
Total	89	5072				5992.8				5382.4			

<sup>a</sup> Sum of Square: sums of squares, sum of the squared differences between the average values and the overall mean.

<sup>b</sup> Degree of freedom.

<sup>c</sup> Mean of Square: Sum of squares divided by Df.



**Table 6.** Comparison of 15 neurons in the hidden layer for removal efficiency by ANN model development with the Levenberg–Marquardt algorithm for MB, BG and CV.

Number of neurons	MB				BG				CV			
	MSE-train	R <sup>2</sup> -train	MSE-test	R <sup>2</sup> -test	MSE-train	R <sup>2</sup> -train	MSE-test	R <sup>2</sup> -test	MSE-train	R <sup>2</sup> -train	MSE-test	R <sup>2</sup> -test
1	0.005421	0.923908	0.002822	0.973670	0.011771	0.902116	0.007638	0.941098	0.007594	0.942125	0.005523	0.913488
2	0.002228	0.987987	0.002132	0.983070	0.005642	0.957703	0.004329	0.975880	0.008594	0.912345	0.003315	0.963331
3	0.001753	0.988195	0.002382	0.974333	0.001973	0.990307	0.003541	0.978176	0.003980	0.965908	0.005369	0.959400
4	0.001337	0.991838	0.001710	0.984631	0.001204	0.997766	0.003013	0.968932	0.004247	0.972391	0.005351	0.932014
5	0.000505	0.998696	0.001199	0.990081	0.000825	0.998840	0.002274	0.980862	0.002209	0.984881	0.003150	0.975245
6	0.000334	0.999628	0.000982	0.986712	0.000784	0.998331	0.001657	0.988000	0.001175	0.995872	0.002449	0.981416
7	0.001172	0.995788	0.001748	0.982144	0.001021	0.995697	0.001314	0.985952	0.000853	0.996699	0.001716	0.976121
<b>8</b>	0.000273	0.999308	0.000527	0.995920	0.001021	0.999335	0.001922	0.983160	0.001147	0.998017	0.002499	0.957441
9	0.000309	0.999623	0.000654	0.993499	0.000940	0.994659	0.001551	0.985281	0.001069	0.995633	0.001757	0.983291
10	0.000367	0.999690	0.001064	0.993552	0.001459	0.995298	0.002652	0.975787	0.001039	0.998368	0.002023	0.974791
11	0.000350	0.999476	0.000677	0.992291	0.001867	0.989616	0.001742	0.986888	0.002911	0.994962	0.003929	0.967318
<b>12</b>	0.000336	0.999568	0.000868	0.994985	0.000826	0.999121	0.001236	0.998146	0.001461	0.992040	0.001763	0.960691
<b>13</b>	0.000979	0.999627	0.001032	0.991068	0.000915	0.998520	0.001844	0.983562	0.000826	0.998468	0.001290	0.985087
14	0.000572	0.999857	0.000878	0.988946	0.001298	0.991514	0.001259	0.990562	0.001269	0.998376	0.001885	0.980868
15	0.000608	0.999721	0.001551	0.979541	0.000901	0.999283	0.001636	0.985598	0.001528	0.997022	0.002018	0.982561

**Table 7.** Isotherm constant parameters and correlation coefficients calculated for the adsorption of dyes onto MnO<sub>2</sub>-NP-AC in single component system.

Isotherm	Parameters	Dye											
		CV				BG				MB			
		0.005 g	0.010 g	0.015 g	0.022 g	0.005 g	0.010 g	0.015 g	0.022 g	0.005 g	0.010 g	0.015 g	0.022 g
Langmuir	Q <sub>m</sub> (mg.g <sup>-1</sup> )	263.16	148.81	108.23	86.66	206.20	147.27	94.69	68.82	234.20	141.83	95.51	74.02
	K <sub>L</sub> (L mg <sup>-1</sup> )	0.874	4.048	4.666	3.746	0.976	4.140	8.874	8.117	2.160	3.890	7.425	5.774
	R <sup>2</sup>	0.995	0.995	0.999	0.995	0.999	0.995	0.999	0.998	0.996	0.999	0.997	0.999
	R <sub>L</sub>	0.0367- 0.1862	0.0082- 0.0471	0.0071- 0.0411	0.0088- 0.0507	0.0330- 0.1701	0.0080- 0.0461	0.0037- 0.0220	0.0041- 0.0240	0.0152- 0.0847	0.0085- 0.0489	0.0045- 0.0262	0.0057- 0.0335
	χ <sup>2</sup>	0.1079	0.1544	0.1911	0.0541	0.0723	0.4029	0.0535	0.1004	0.0620	0.1002	0.1978	0.0478
Freundlich	1/n	0.445	0.385	0.569	0.644	0.379	0.380	0.4688	0.514	0.336	0.486	0.475	0.565
	K <sub>F</sub> (L mg <sup>-1</sup> )	7.637	7.688	7.928	7.313	7.018	7.65	7.804	7.017	8.471	7.986	7.614	7.060
	R <sup>2</sup>	0.972	0.982	0.969	0.986	0.927	0.975	0.958	0.974	0.975	0.962	0.972	0.973
	χ <sup>2</sup>	1.2852	1.1234	1.0113	0.8462	1.5695	1.1229	1.0096	0.8759	1.2317	1.1420	1.0120	0.8582
Temkin	B	52.85	25.66	23.47	17.93	43.31	22.036	19.445	14.50	37.34	29.65	19.54	15.93
	K <sub>T</sub> (L mg <sup>-1</sup> )	10.63	76.21	47.93	42.35	10.27	79.08	100.08	88.69	54.38	42.61	85.30	60.25
	R <sup>2</sup>	0.994	0.978	0.994	0.984	0.984	0.987	0.990	0.991	0.994	0.998	0.995	0.995
	χ <sup>2</sup>	0.1406	0.3574	0.1754	0.2276	0.1292	0.1929	0.1326	0.1843	0.078	0.1513	0.1425	0.1421
Dubinin- radushkevich	Q <sub>s</sub> (mg g <sup>-1</sup> )	186.3	94.38	86.84	65.04	156.5	98.69	86.20	61.07	174.0	115.4	83.56	63.18
	β×10 <sup>-8</sup>	7.190	1.550	2.370	2.540	9.210	1.810	1.850	1.900	2.710	2.800	1.940	2.310
	E (kJ mol <sup>-1</sup> )	2.637	5.679	4.652	6.274	2.329	5.255	5.198	7.254	4.295	5.226	5.077	6.579
	R <sup>2</sup>	0.907	0.961	0.980	0.972	0.928	0.984	0.986	0.983	0.937	0.984	0.981	0.975
	χ <sup>2</sup>	2.4415	1.8350	1.6036	1.7303	2.2308	1.6564	1.5032	1.6532	1.9397	1.4639	1.8026	1.6895

**Table 8.** Kinetic parameters for the adsorption of dyes using 0.01 g of MnO<sub>2</sub>-NP-AC as well as 10, 20 and 30 mg L<sup>-1</sup> of each dye in single component system.

Model	Parameters	Value of parameters								
		CV			BG			MB		
		Concentration (mg L <sup>-1</sup> )								
	10	20	30	10	20	30	10	20	30	
Pseudo-First-order- kinetic	k <sub>1</sub> (min <sup>-1</sup> )	0.0134	0.0129	0.0230	0.0145	0.0124	0.0128	0.0163	0.0239	0.0242
	q <sub>e</sub> (calc) (mg g <sup>-1</sup> )	15.977	18.093	46.830	11.855	16.807	18.634	7.888	30.960	31.320
	R <sup>2</sup>	0.960	0.981	0.975	0.968	0.977	0.818	0.977	0.876	0.970
	χ <sup>2</sup>	2.5510	1.7113	0.9721	1.5913	1.6527	2.9861	0.8546	1.6639	0.7212
Pseudo-second-order-kinetic	k <sub>2</sub> (min <sup>-1</sup> )	0.0015	0.0015	0.0014	0.0111	0.0016	0.0003	0.0044	0.0022	0.0021
	q <sub>e</sub> (calc) (mg g <sup>-1</sup> )	51.282	101.01	149.25	48.544	93.340	135.14	50.080	98.039	140.85
	R <sup>2</sup>	0.999	0.999	0.996	0.999	0.999	0.999	0.999	0.999	0.999
	χ <sup>2</sup>	0.01392	0.0075	0.0120	0.0094	0.0132	0.0203	0.0044	0.0088	0.0067
Intraparticle diffusion	K <sub>dif</sub> (mg g <sup>-1</sup> min <sup>-1/2</sup> )	0.807	1.018	1.790	0.557	0.918	0.674	0.412	0.843	0.600
	C (mg g <sup>-1</sup> )	35.950	82.841	118.45	38.335	77.477	122.98	42.922	83.274	130.43
	R <sup>2</sup>	0.943	0.902	0.661	0.900	0.926	0.950	0.810	0.730	0.834
	χ <sup>2</sup>	0.37652	0.4079	1.3309	0.2236	0.3314	0.8511	0.3462	1.0440	0.7058
Elovich	β (mg g <sup>-1</sup> min <sup>-1</sup> )	0.233	0.239	0.253	0.332	0.293	0.295	0.430	0.489	0.310
	α (g mg <sup>-1</sup> )	134.66	412.70	630.91	127.63	335.12	521.68	139.37	283.27	536.18
	R <sup>2</sup>	0.949	0.960	0.958	0.980	0.992	0.973	0.920	0.942	0.931
	χ <sup>2</sup>	0.34107	0.6144	0.5789	0.1391	0.1001	0.4136	0.2281	0.7522	0.6337
Experimental data	q <sub>e</sub> (exp) (mg g <sup>-1</sup> )	48.90	99.09	145.26	47.22	92.30	133.40	49.32	96.22	139.10

**Table 9.** Validation and comparison of experimental data set.

Optimization runs for RSM and ANN models																						
	Factors						Experimental values			RSM predicted			ANN predicted			Absolute error						
																RSM			ANN			
	X <sub>1</sub>	X <sub>2</sub>	X <sub>3</sub>	X <sub>4</sub>	X <sub>5</sub>	X <sub>6</sub>	%R MB	%R BG	%R CV	%R MB	%R BG	%R CV	%R MB	%R BG	%R CV	MB	BG	CV	MB	BG	CV	
1	7.0	0.022	4.0	6.0	6.0	6.0	96.64	99.40	95.15	100.74	101.21	97.86	99.78	100.68	96.76	4.10	1.81	2.71	0.38	1.28	1.61	
2	7.0	0.022	4.0	6.0	6.0	6.0	97.86	98.87	94.70	100.74	101.21	97.86	99.78	100.68	96.76	2.88	2.34	3.16	0.91	1.81	2.06	
3	7.0	0.022	4.0	6.0	6.0	6.0	99.43	96.30	96.62	100.74	101.21	97.86	99.78	100.68	96.76	1.31	4.91	1.24	3.48	4.38	0.14	
4	7.0	0.022	4.0	6.0	6.0	6.0	98.35	97.53	97.90	100.74	101.21	97.86	99.78	100.68	96.76	2.39	3.68	-0.04	2.25	3.15	-1.14	
5	7.0	0.022	4.0	6.0	6.0	6.0	99.12	95.41	96.23	100.74	101.21	97.86	99.78	100.68	96.76	1.62	5.80	1.63	4.37	5.27	0.53	
6	7.0	0.022	4.0	6.0	6.0	6.0	97.98	98.72	92.77	100.74	101.21	97.86	99.78	100.68	96.76	2.76	2.49	5.09	1.06	1.96	3.99	
Average							<b>98.23</b>	<b>97.71</b>	<b>95.56</b>	<b>100.74</b>	<b>101.21</b>	<b>97.86</b>	<b>99.78</b>	<b>100.68</b>	<b>96.76</b>	<b>2.51</b>	<b>3.50</b>	<b>2.30</b>	<b>2.08</b>	<b>2.98</b>	<b>1.20</b>	
RSM and ANN predictions for totally unseen data.																						
1	4.3	0.015	2.5	6.9	7.6	6.0	87.50	88.21	81.61	89.80	89.80	83.22	88.98	88.72	82.02	2.3	1.59	1.61	1.48	0.51	0.41	
2	7.9	0.028	3.7	7.8	4.5	7.8	94.62	93.25	98.10	96.10	95.30	99.80	95.85	94.76	99.43	1.48	2.05	1.7	1.23	1.51	1.33	
3	5.2	0.027	5.0	6.0	7.0	6.0	89.76	93.70	88.32	91.70	96.40	90.00	90.65	95.32	89.67	1.94	2.7	1.68	0.89	1.62	1.35	
4	9.0	0.023	5.1	6.4	6.1	4.7	96.33	95.11	97.87	99.10	96.40	99.90	98.23	98.12	96.25	2.77	1.29	2.03	1.9	3.01	-1.62	
5	7.6	0.020	5.7	6.2	6.6	4.2	99.12	96.34	93.67	98.20	99.80	96.00	99.67	98.20	94.11	-0.92	3.46	2.33	0.55	1.86	0.44	
6	6.5	0.018	4.8	4.0	6.7	4.4	98.25	96.21	97.42	99.40	99.50	98.90	98.90	98.34	96.50	1.15	3.29	1.48	0.65	2.13	-0.92	
7	8.7	0.010	5.3	7.7	7.6	5.2	72.24	83.24	82.68	75.60	85.48	81.66	74.32	83.78	84.34	3.36	2.24	-1.02	2.08	0.54	1.66	
8	4.4	0.020	1.5	4.8	4.0	7.9	83.78	76.34	75.21	85.68	78.17	77.02	84.25	77.42	77.49	1.9	1.83	1.81	0.47	1.08	2.28	
9	4.3	0.020	2.0	2.4	4.1	10.6	79.31	77.11	59.42	81.13	78.40	62.3	81.12	78.54	61.23	1.82	1.29	2.88	1.81	1.43	1.81	
10	6.0	0.013	6.8	11.5	4.1	3.3	55.43	70.98	75.01	60.21	73.91	77.85	58.87	72.43	76.49	4.78	2.93	2.84	3.44	1.45	1.48	
																<b>2.06</b>	<b>2.27</b>	<b>1.73</b>	<b>1.45</b>	<b>1.51</b>	<b>0.82</b>	
Appraisal of ANN and RSM models							R			R <sup>2</sup>			AAD			MAE			RMS			
Response							MB	BG	CV	MB	BG	CV	MB	BG	CV	MB	BG	CV	MB	BG	CV	
RSM (n=10 runs)							0.9975	0.9968	0.9964	0.9951	0.9937	0.9928	2.608	2.541	2.083	0.0341	0.0267	0.0253	0.0280	0.0254	0.0233	
ANN (n=10 runs)							0.9991	0.9978	0.9969	0.9983	0.9957	0.9938	1.850	1.686	1.098	0.0185	0.0169	0.0212	0.0239	0.0182	0.0257	
RSM (n=90 runs)							0.9985	0.9965	0.9935	0.9970	0.9930	0.9870	0.4162	0.5909	0.7601	0.3703	0.5250	0.6709	0.4388	0.6871	0.8540	
ANN (n=90 runs)							0.9965	0.9970	0.9950	0.9930	0.9940	0.9900	0.4518	0.4518	0.6202	0.4086	0.4775	0.5510	0.6315	0.6355	0.7522	

**Table 10.** Comparison for the adsorption of dyes by different methods and adsorbents.

Adsorbent	dye	pH	Sorption capacity (mg g <sup>-1</sup> )	Contact time (min)	Ref.
Coniferous Pinus Bark (CPBP)	CV	8.0	32.78	120	52
Tomato Plant Root (TPR powder)	CV	6.7	94.34	15	53
Wood Apple Shell (W-AS)	CV	10.0	129.90	120	54
Grapefruit Peel (GFP)	CV	6.0	254.20	60	6
Wheat Straw (EWS)	CV	4.0	227.30	300	55
Treated Ginger Waste (TGW)	CV	9.5	277.70	150	56
Palm Kernel Fiber (PKF)	CV	7.2	78.90	60	57
Soil-Silver Nanocomposite (soil-AgNP)	CV	4.7	1.92	30	13
Magnetic Nanocomposite	CV	8.50	113.31	30	58
Magnetic Calcium Ferrite Nanoparticle CaFe <sub>2</sub> O <sub>4</sub>	CV	5.0	10.67	30	59
MnO <sub>2</sub> -NPs-AC	CV	7.0	263.16	4.0	This work
Zinc oxide nanoparticles loaded on -AC	BG	5.0	142.90	35	60
pine-fruit shell by chemically AC	BG	5.5	219.10	240	61
pine-fruit shell by chemically and physically AC	BG	5.5	263.40	240	61
Surfactant modified nano- $\gamma$ -alumina	BG	4.0	168.59	50	62
Surfactant Doped Polyaniline/MWCNTs Composite	BG	3.0	476.19	240	63
graphite oxide nanoparticle (GO-NP)	BG	7.0	232.56	14	8
graphite oxide nanoparticle (GO-NP)	BG	7.0	416.67	10	10
Ruthenium nanoparticles -AC (Ru-NP-AC)	BG	6.0	94.70	45	19
MnO <sub>2</sub> -NPs-AC	BG	7.0	206.20	4.0	This work
MWCNTs filled with Fe <sub>2</sub> O <sub>3</sub> particles	MB	6.0	42.90	60	64
Activated carbon (walnut shells)	MB	7.0	315.00	1440	65
Ag NPs-AC	MB	2.5	71.43	15	66
Au-NP-AC	MB	7.0	185.00	1.6	67
Graphene	MB	10.0	153.85	255	68
PDA microspheres	MB	6.5	90.70	100	69
Fe <sub>3</sub> O <sub>4</sub> nanoparticles	MB	6.0	89.20–91.90	2	70
Humic Acid-coated Fe <sub>3</sub> O <sub>4</sub> -NP (HA-Fe <sub>3</sub> O <sub>4</sub> )	MB	8.4	93.08	27	11
NiS-NP-AC	MB	8.1	46–52	5.46	71
CuO-NP-AC	MB	7.0	10.55	15	12
MnO <sub>2</sub> -NPs-AC	MB	7.0	234.20	4.0	This work

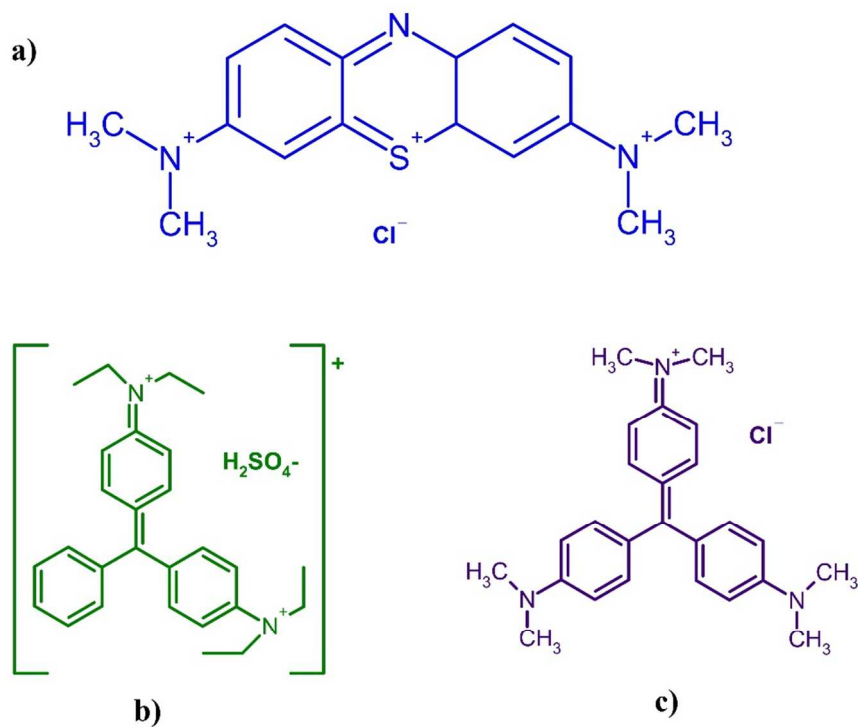


**Fig. 1.** Chemical structure of (a) MB, (b) BG and (c) CV.

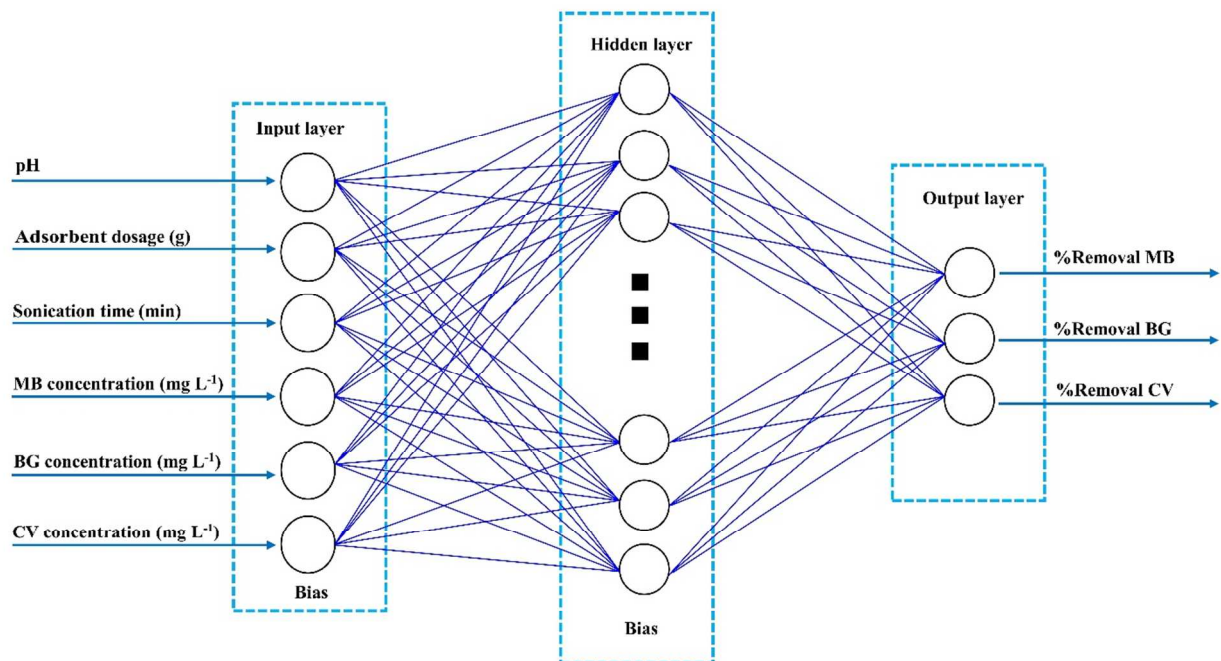


**Fig. 2.** Simple illustration of ANN structure and basic principles of ANN.

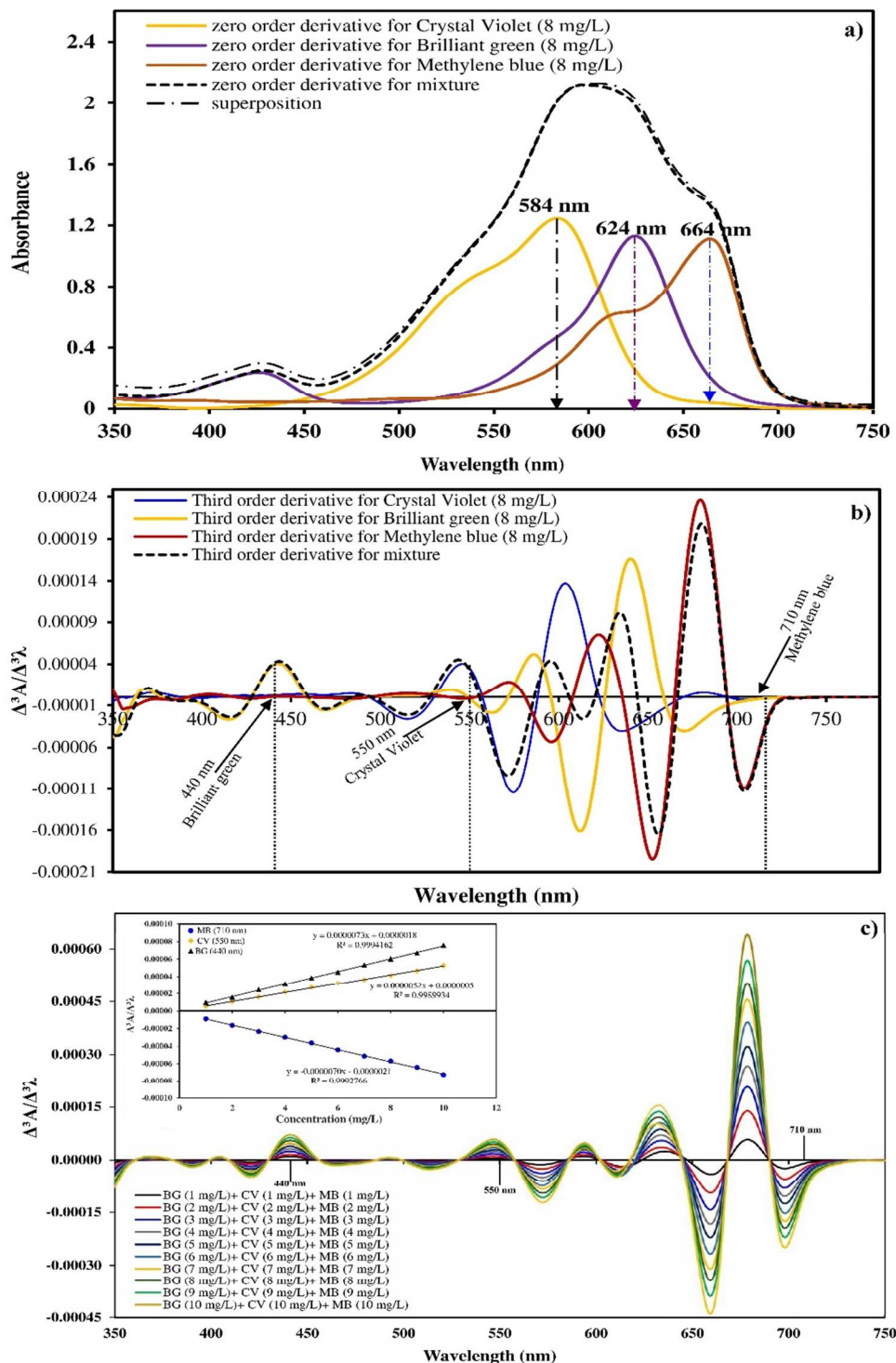


**Fig. 3.** a) Zero order absorption spectra of CV, BG and MB in single and ternary solutions (Initial dye concentration of 8 mg/L for each dye). b) Third order derivative spectra of CV, MG and MB in ternary solutions and c) calibration graph at 710 nm for MB, 550 nm for CV and 440 nm for BG.



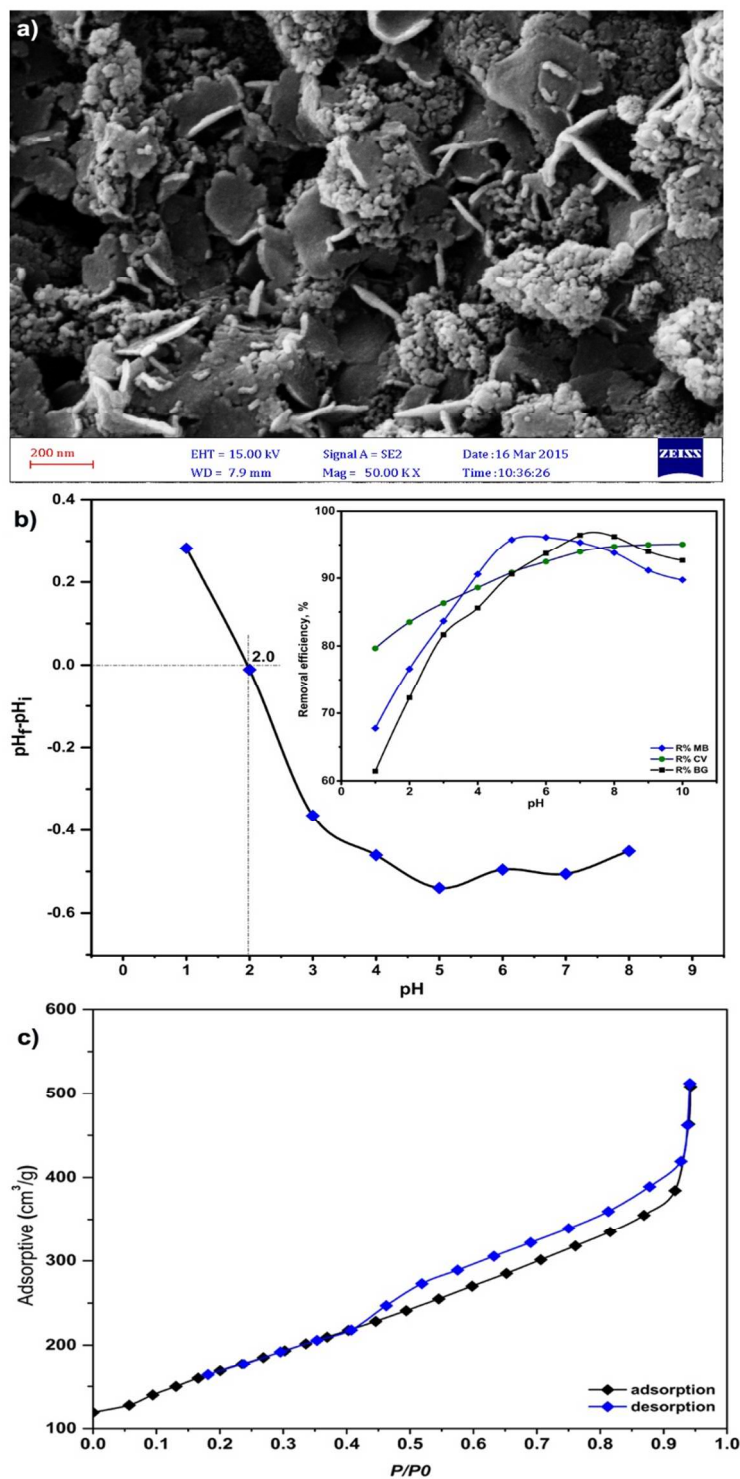


**Fig. 4.** a) FESEM image of the prepared MnO<sub>2</sub>-NP-AC, b) pHzpc of MnO<sub>2</sub>-NP-AC (pH<sub>i</sub>=initial pH and pH<sub>f</sub>=final pH) and c) Nitrogen adsorption-desorption isotherms.

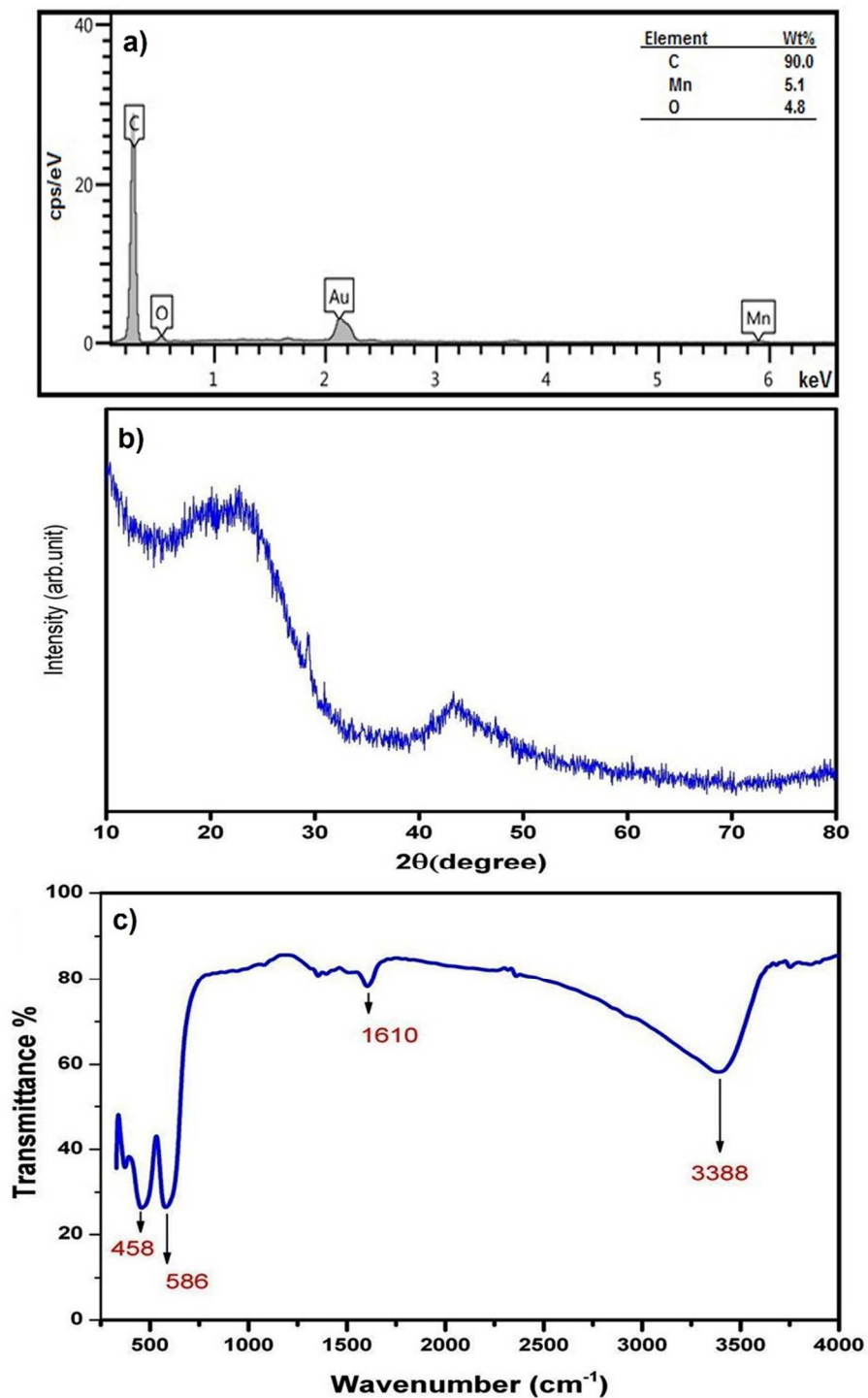


**Fig. 5.** a) EDX analysis, b) XRD pattern and c) FTIR spectrum of MnO<sub>2</sub>-NP-AC.

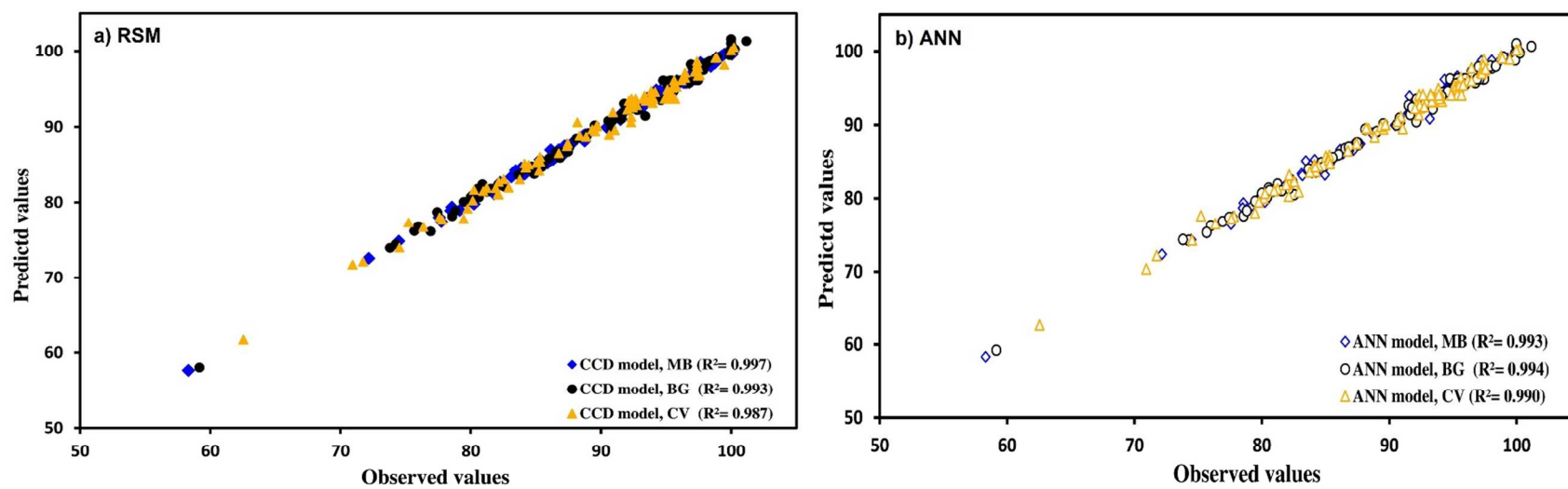


**Fig. 6.** Predicted vs. experimental data for dyes using **a)** RSM and **b)** ANN

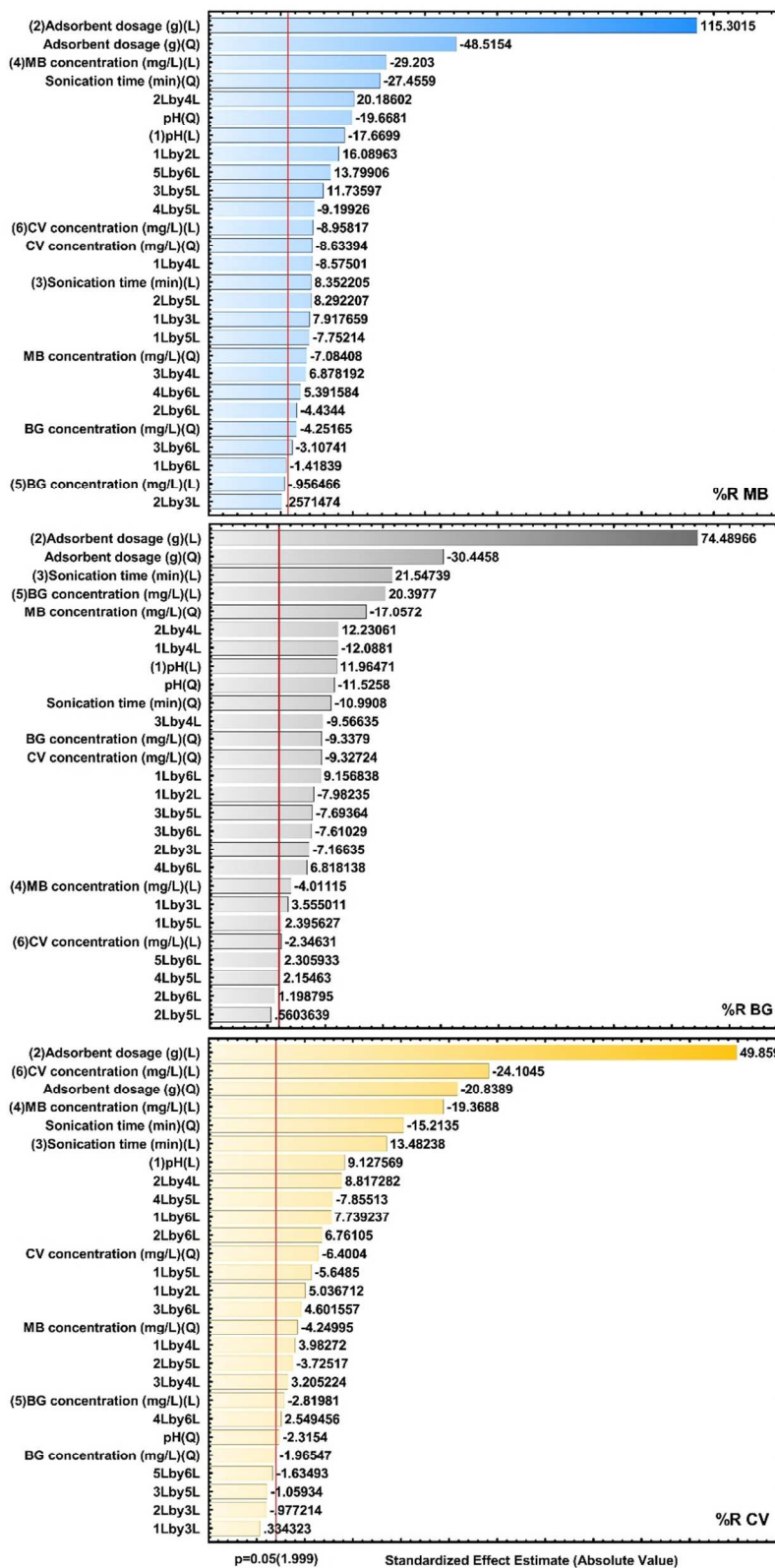
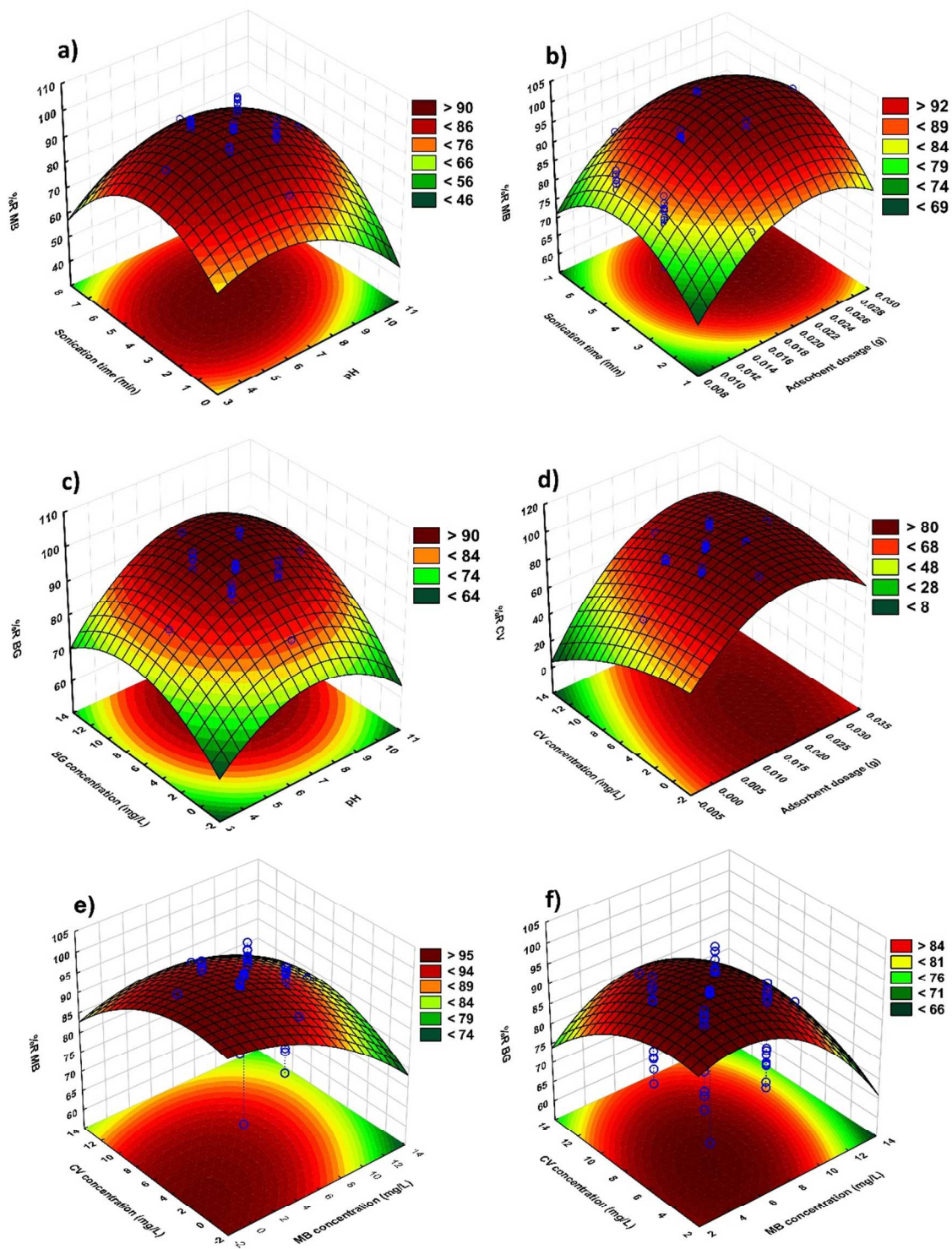
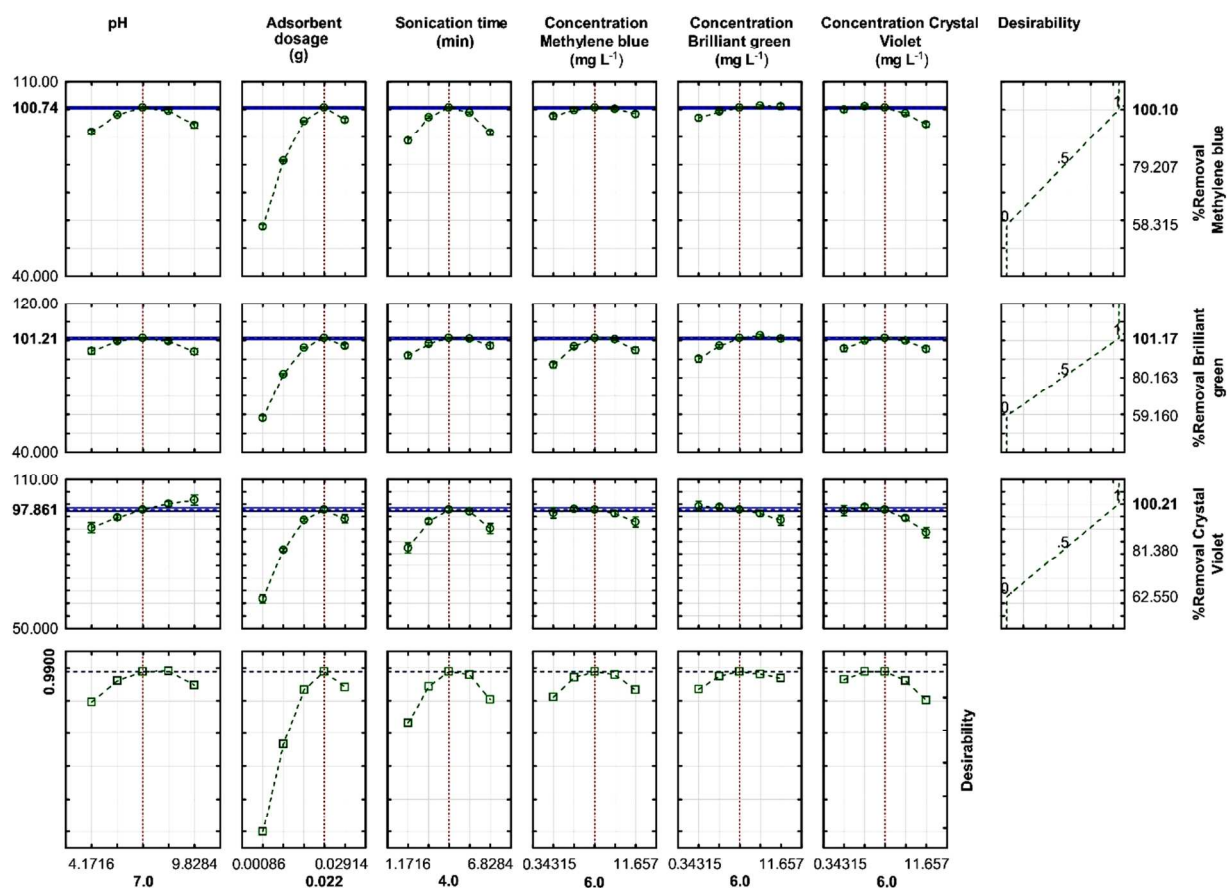


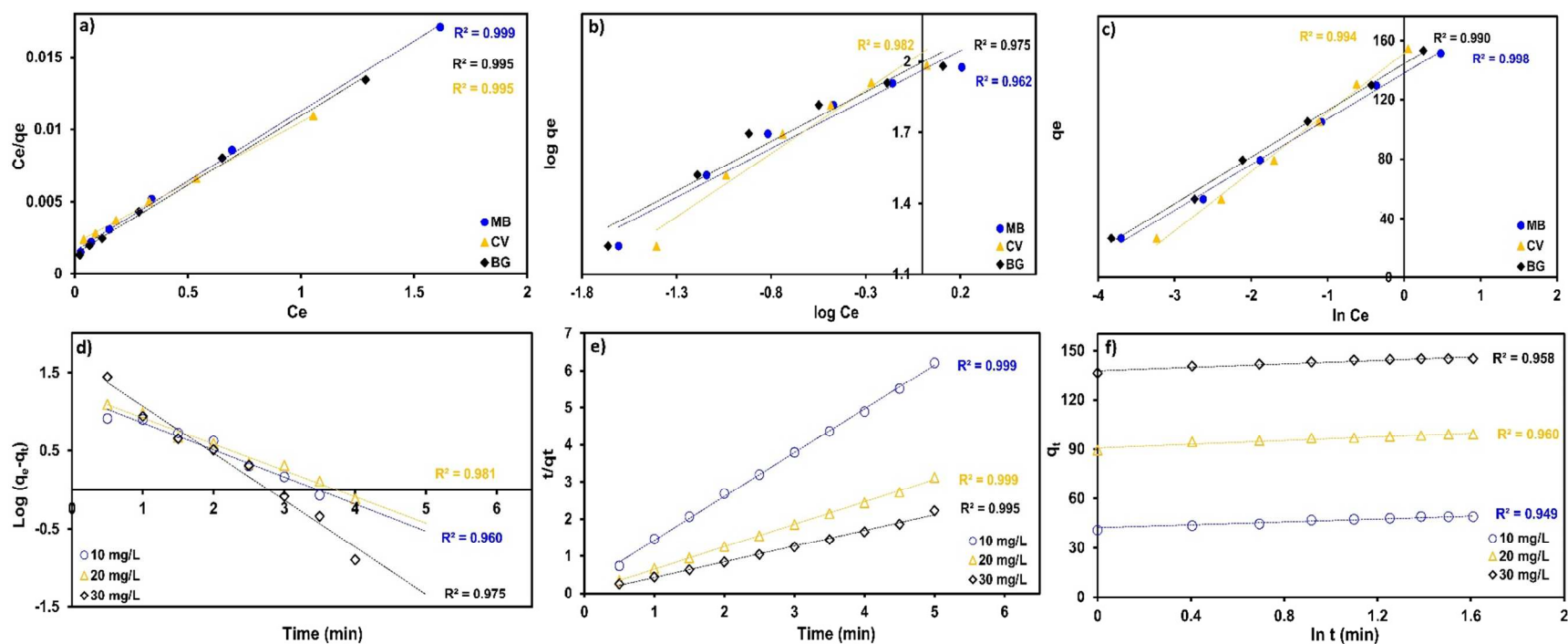
Fig. 7. Standardized main effect Pareto chart for the removal of MB, BG and CV using CCD.



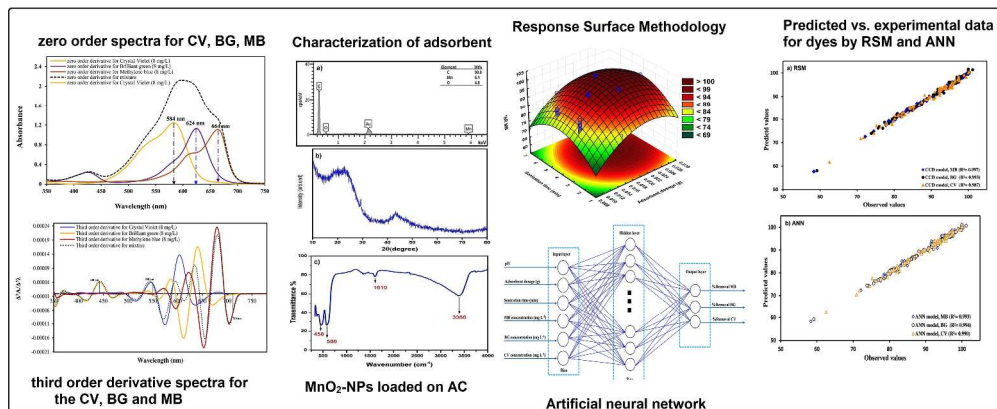
**Fig. 8.** 3D response surfaces: **a)** pH–Sonication time (MB); **b)** adsorbent dosage–Sonication time (MB); **c)** pH–BG concentration (BG); **d)** CV concentration – adsorbent dosage (CV); **e)** CV concentration – MB concentration (MB) and **f)** CV concentration – MB concentration (BG).



**Fig. 9.** Profiles for predicted values and desirability function for removal percentage of MB, BG and CV. Dashed lines indicate the current values after the optimization.



**Fig. 10.** Data obtained for dyes adsorption onto  $\text{MnO}_2\text{-NP-AC}$  at different initial concentrations of dyes and to determine isotherm parameters **a)** Langmuir, **b)** Freundlich and **c)** Temkin ( $C_0=5\text{-}30\text{ mg L}^{-1}$ , adsorbent dosage= $0.01\text{ g}$ , sonication time= $4\text{ min}$ ,  $\text{pH}=7.0$ ), **d)** pseudo-first order, **e)** pseudo-second-order kinetic and **f)** Elovich plots for CV adsorption onto  $\text{MnO}_2\text{-NP-AC}$ .



2003x835mm (72 x 72 DPI)